MODIFIED COMBINED VECTOR AND DIRECT POWER CONTROL FOR DFIG-BASED WIND TURBINES USING ADAPTIVE PID CONTROLLER

BY

ALI AMEEN BALFAS

A Thesis Presented to the
DEANSHIP OF GRADUATE STUDIES

KING FAHD UNIVERSITY OF PETROLEUM & MINERALS

DHAHRAN, SAUDI ARABIA

In Partial Fulfillment of the
Requirements for the Degree of

MASTER OF SCIENCE

In

ELECTRICAL ENGINEERING

March 2019

KING FAHD UNIVERSITY OF PETROLEUM & MINERALS

DHAHRAN- 31261, SAUDI ARABIA

DEANSHIP OF GRADUATE STUDIES

This thesis, written by **ALI AMEEN ALI BALFAS** under the direction of his thesis

advisor and approved by his thesis committee, has been presented and accepted by the

Dean of Graduate Studies, in partial fulfillment of the requirements for the degree of

MASTER OF SCINCE IN ELECTRICAL ENGINEERING.

Dr. Mahmoud Kassas
(Advisor)

Dr. Abdallah S. Al-Ahmari
Department Chairman

Dr. Mohammad Khalid
(Member)

Dr. Salam A. Zummo
Dean of Graduate Studies

Dr. Hussain N. Al-Duwaish
(Member)

10/11/19

Date

This Thesis is dedicated to my supportive father,

my loving mother, my brothers, my wife, my kids

and all my friends

ACKNOWLEDGMENTS

I would first like to thank my thesis advisor Dr. M. Kassas, for his guidance, his help, his patience and his encouragement.

I would also like to express my appreciation to my thesis committee Dr. Mohammad Khalid and Dr. Hussain N. AL-Duwaish, for their directions and cooperation.

Many thanks to King Fahd University of Petroleum and Minerals (KFUPM) and the Hadhramout Establishment for Human Development (HEHD) for giving me the chance to pursue the master's program.

Finally, I must express My heart-felt gratitude to my family for their continuous support and their endless encouragement throughout my years of study. Without them, this accomplishment would not have been possible.

TABLE OF CONTENTS

LIST OF TABLES

LIST OF FIGURES

LIST OF ABBREVIATIONS

DPC   Direct Power Control

VC   Vector Control

DFIG   Doubly Fed Induction Generator

WT   Wind Turbine

CVDPC   Combined Vector and Direct Power Control

GSC   Grid Side Converter

RSC   Rotor Side Converter

DTC   Direct Torque Control

PID   Proportional-Integral-Derivative

MPPT   Maximum Power Point Tracking

MRAC   Model Reference Adaptive Control

MG   Micro-Grid

ABC   Artificial Bee Colony Algorithm

SFOF   Stator Flux-Oriented Frame

SVOF   Stator Voltage-Oriented Frame

PLL   Phase Locked- Loop

MRAC   Model Reference Adaptive Control

LSM   Least Square Method

PWM   pulse width modulation

LIM   Linear induction motor

ABSTRACT

Full Name   : ALI AMEEN ALI BALFAS

Thesis Title   : MODIFIED COMBINED VECTOR AND DIRECT POWER
CONTROL FOR DFIG-BASED WIND TURBINES USING
ADAPTIVE PID CONTROLLER

Major Field   : ELECTRICAL ENGINEERING

Date of Degree : MARCH, 2019

A combined vector and direct power control (CVDPC) is carried out for the rotor side converter (RSC) of doubly fed induction generator (DFIGs). This control method is concentrating on a control of direct current by using a switching table to determine and choose suitable voltage. Actually, the performed CVDPC attains the advantages of direct power control (DPC) and vector control (VC) in a combined control system. Its advantage comparing with DPC, include power ripple in lower level and lower harmonic distortion. Likewise, it has advantages comparing with VC including rapid dynamic responses, robustness against parameters variation of the machine, simple implementation and lower computation. On other hand, the use of conventional (PI) controller in VC is necessary in order to guarantee the stability of system even though it will affect the quality of performance of the system. So, in this work, a conventional and adaptive (PID) controllers are applied instead of the performed PI controller to enhance the system performance. The simulation part has been achieved on MATLAB/Simulink and it is done using a 9-MW

wind system (six 1.5-MW wind turbines DFIG-based). The performance of the CVDPC system with conventional PI and PID controller is compared with the proposed modified CVDPC system with adaptive PID controller under steady-state and robustness conditions against parameters variation.

Keywords: Direct power control DPC, doubly fed induction generator DFIG, vector control VC, wind turbine WT, combined vector and direct power control CVDPC.

ملخص الرسالة

الاسـم الكـــامل : **علي أمين علي بلفاس.**

عنوان الرســالة : **المتحكم المركب من متحكم متجه الفولتية و متحكم الطاقة المباشر المستخدم للتحكم بالمولد الحثي ثنائي التغذية المستخدم في التوربينات الهوائية والمعدل باستخدام المتحكم التناسبي ــ التفاضلي ـالتكاملي الثابت والمتكيف لحظياً.**

التخـــصص : **هندسة كهربائية.**

تاريخ الدرجة العلمية: مارس، **2019.**

للتحكم في المولد الحثي ثنائي التغذية فقد تم استخدام متحكم مركب من متحكم متجه الفولتية مع آخر يدعى متحكم الطاقة المباشرة حيث انهما يتميزان بكثير من المميزات والتي تجعل من النظام يعمل بكفاءة عالية. ولكن خلال هذا المتحكم يتم استخدام متحكم آخر يسمى المتحكم التناسبي-التفاضلي-التكاملي الثابت بحيث يعمل على الحفاظ على كفاءة وثبات المولد على الرغم من انه سيؤثر على جودة ومخرجات المتحكم المركب المذكور آنفاً.

في هذه الرسالة تم استبدال المتحكم التناسبي-التفاضلي بالمتحكم التناسبي-التفاضلي-التكاملي الثابت ومن ثم بالمتحكم التناسبي-التفاضلي-التكاملي المتكيف لحظياً للتخلص من هذه السلبية. نتائج المحاكاة تظهر أفضلية وحدة التحكم المقترحة (المتحكم المركب من متحكم متجه الفولتية ومتحكم الطاقة المباشر المستخدم للتحكم بالمولد الحثي ثنائي التغذية والمعدل باستخدام المتحكم التناسبي-التفاضلي-التكاملي الثابت والمتكيف لحظياً) مقارنةً باستخدام نفس المتحكم والمستخدم معه المتحكم التناسبي-التفاضلي الثابت.

CHAPTER 1

INTRODUCTION

A long time ago, the demand of electrical power has been increasing enormously and depletion of resources in nature has increased energy and environmental crises. Wherefore, the need of using renewable resources to produce energy has been arising so, the energy production of world wind has expanded rapidly because of renewability and cleanness. The generation of wind power is expected to be around 10% of the total electricity all over the world by the end of 2020 and it is predicted to be more than the double by the year 2040. The wind energy main role is wind turbines WTs. These WTs are essentially classified into variable and fixed speed strategies. Variable speed wind turbines have been rapidly utilized lately due to some benefits compared to the fixed-speed turbines, such as maximizing power generation, minimized mechanical stress imposed on the turbines, enhanced the quality of power generated, and minimized acoustical noise [1].

The technologies of variable speed-based wind turbines are also divided into two sorts: full-scale converter synchronous generators and partial-scale converter DFIGs. DFIGs are specially applied for high scale systems, because of the minimum power losses and converters cost. The DFIGs control includes grid side converter (GSC) and rotor side converter (RSC) controllers, hence, RSC controls both stator active power and reactive power, and the GSC produces an independent reactive power and in same time regulates

dc-link voltage that is forwarded into the grid [2]. VC is the widespread technique applied on the DFIG wind turbines WTs [3], [4].

Its features include minimum converter switching frequency, an accurate performance of steady-state, and lower power ripple. Nevertheless, VC has some demerits, like its reliance on variation of machine parameters because of the decoupling conditions and high on-line computations owing to the pulse width modulation (PWM) method. Furthermore, the PI controller coefficients, in the classical vector control VC, must be tuned optimally to ensure the stability of the system within the entire operating domain and to get appropriate dynamic responses through the transient conditions [5].

These disadvantages may affect the transient performances of VC and deteriorate the stability of the system during changing operation conditions. So, to avoid the aforementioned issues, various nonlinear control techniques like direct power control/direct torque control (DPC/DTC) have been suggested [6], [7].

The main benefits of DPC/DTC techniques including rapid dynamic responses, robustness against the variation of machine parameters, simple implementation and lower computation. On the other hand, these methods have some disadvantages such as large power/torque ripples because of the hysteresis controllers' bandwidth is high, converters' variable switching frequency, and decadence of the performance of controller within the starting of the machine and low-speed operations. Hence, many modified techniques have been proposed to fix these issues [8]– [10].

To gain the advantages of both VC and DPC, the combined of both methods results CVDPC technique which has been introduced successfully in permanent magnet

synchronous motor [11], [12] and induction motors [13]–[15]. However, the CVDPC technique has been investigated recently for the DFIGs. The CVDPC technique is applied for the RSC of DFIGs. This technique has many merits comparing to vector control VC, such as rapid dynamic responses, robustness against the variation of machine parameters, simple implementation and lower computations. Also, it has merits comparing to direct power control DPC, such as, power ripple in lower level and lower harmonic distortion.

1.1 Problem Statement

The DFIG wind turbines are the most popular generation used in wind power production due to several merits including providing simple pitch control, cost effective, enhancing system efficiency, and maximizing the output power. So, the need for simple and effective control strategies has been raised.

The CVDPC system is applied for the RSC of DFIG. The system consists of two different control techniques, VC and DPC controllers combined together. The performed CVDPC attains the advantages of both DPC and VC such as, rapid dynamic responses, robustness against the variation of machine parameters, simple implementation, lower computation and lower harmonic distortion.

However, the PI controller coefficients, in the conventional vector control VC, should be tuned in optimal fashion to guarantee the stability of system during the entire range of operation and to achieve appropriate dynamic responses within the transient conditions [5]. This will affect the transient performances of vector control VC and will impact the performance quality of system during operation condition variations.

3

1.2   Thesis Objectives

- Design and development of conventional and adaptive PID controller on CVDPC DFIG- based.

- Investigate the performance of CVDPC DFIG- based **using conventional PID controller**.

- Investigate the performance of CVDPC DFIG- based **using adaptive PID controller.**

- Compare the performances of the system according to CVDPC conventional PI, conventional PID and adaptive PID controller based.

1.3   The Work Contribution

- Enhancing the power fluctuating under steady state condition.

- Enhancing the behavior of the system in presence of disturbances and parameter changing.

- Guarantee the robustness of the system during disturbances.

1.4 Thesis Outlines

The work is divided into five parts as following:

Chapter 1: **INTRODUCTION**

Introduces the problem of steady state and transient stability as a major issue in the control of wind turbines DFIG-based systems. Additionally, the problem formulation, basic objectives of the study and thesis outlines are briefly discussed.

Chapter 2: LITERATURE REVIEW

Indicates the related work that has been done in the literature to address this problem.

Chapter 3: METHODOLOGY

Represents the methodology of the thesis by showing the thesis steps and modulation.

Chapter 4: **SIMULATION RESULTS AND DISSCUSION**

The control design has been developed to achieve the objectives of this study and satisfy the constraints of the system.

Chapter 5: CONCOLUSION

The work is concluded, and the results are summarized.

CHAPTER 2

LITERATURE REVIEW

Linear induction motors (LIMs) control system is proposed to attain very fast and smooth machine dynamics operation through large operating conditions and the end effects are considering. In addition, it is targeted at a control system similar to the conventional direct torque control DTC or vector control VC in terms of complexity of the system such as requirement of the signal measurement and online computational load.

Moreover, this control system is used in induction motors to minimize loss and torque pulsation minimization control. Also, this technique is used in permanent magnet synchronous machines and then, lately used in (DFIMs) [16].

The wind energy conversion system (WECS) based on a DFIG technology is introduced in [17]. Back to back based power converters are used to control the system. This converter is constructed using a neutral point clamped (NPC) bridges at two three-levels related to a DC bus.

On the other hand, the converter of machine side is controlled using the introduced DTC strategy, and the converter of grid side is controlled using the DPC technique.

Both aforementioned controllers reduce cost function based upon the errors of control variables at every control cycle. The direct power control DPC sources are utilized to handle the DC buses voltage constant, while the direct torque control DTC sources are used

to attain maximum power extracted from the wind, control the stator power factor and ensure the stability of capacitors of the DC bus.

The maximum power point tracking (MPPT) method is applied to establish a torque source by taking in consideration the pitch angle of blade. The proposed wind energy conversion system WECS leads to investigate the rotor dynamic models, power quality behaviors, and control techniques for wide range of wind turbine models.

A new improved mechanism has been introduced in [18] for developing control of a DFIG wind turbine through a direct-current vector control configuration. According to the introduced control mechanism, the unified DFIG control system is constructed, includes reactive power control, maximum wind power extraction control, and grid voltage support control. i.e. a wind turbine DFIG-based control has been studied using a direct-current vector control strategy. The author investigates the introduced control diagram with the conventional DFIG control strategy. Then, he illustrates, according to the proposed above-mentioned control, how the integrated GSC and RSC control is constructed to achieve the dc-link voltage, reactive power, grid voltage support control function, and maximum power extraction.

Another work introduces applications of a reactive power and DTC for DFIG grid-connected-based in wind power generation. The suggested direct torque control DTC technique utilizes a variable structure control (VSC) design to determine the desired rotor control voltage instantly and to vanish the instantaneous error of both active power and reactive power without including a synchronous coordinate transformation, which basically improves the transient performances [19].

Furthermore, space vector modulation (SVM) is employed to accomplish the fixed switching frequency, which smooths the design of ac harmonic filter and power converters. This strategy was simulated on a 2MW DFIG grid-connected-based model and was designed and compared with designs of the classic voltage-oriented VC and traditional look-up-table (LUT) DPC.

The suggested variable structure control VSC direct torque control DTC keeps improving transient performances similar to LUT DPC and maintains the harmonic spectra of steady-state at the similar level as the vector control VC technique when the network is precisely balanced.

For doubly fed induction generator DFIG, a robust continuous-time model predictive control (RCTMPC) has been proposed. The presented scheme determines directly the commands of rotor voltage over the synchronous reference frame's predictive stator current [20].

So, depending upon quadratic cost minimization function, the base line controller has been designed and consists of the errors between the stator current references and their components.

A disturbance observer has been combined to RCTMPC to improve the performance of steady-state in the existence of the uncertainties of the model and external disturbances.

The closed-loop model's performances based on the introduced controller are validated experimentally using a DFIG grid-connected-based. The suggested controller supplies precise behavior under synchronous, sub-synchronous, and super-synchronous fashions and, also, works very smoothly under uncertainty of the system.

Furthermore, naturally, an integral action appears in a composite controller instead of being directly applied on the control loop. According to appropriate design factors, as that for the vector control VC technique, a good steady-state and transient performance can be achieved without the presence of an additional current control loop.

A high performance enhanced direct power control DPC based on neuro fuzzy control (NFC) and model reference adaptive control (MRAC) for grid-connected DFIGs, to vanquish the DPC drawbacks that was based only on PID controller, namely the divergence and efficiency/speed trade-off from peak power during wind speed fast variation [21].

A DFIG mathematical model is derived on d-q reference frames. After that, the DPC strategy is used to control the DFIGs' rotor currents employing PID controllers, and to calculate the space-vector modulation SVM, a fixed switching frequency is handled.

Also, the power factor of the stator side condition has been controlled via maximum power point tracking MPPT technique at unity level. The model reference adaptive control MRAC that is based on direct power control DPC is examined rather than PID regulators. Moreover, the performance of neuro fuzzy control NFC based on direct power control DPC are investigated.

Another strategy is introduced in [22], where the goal was to apply a robust control technique for exchanging power between the DFIG rotor and the grid. A voltage source converter is feeding the rotor while the stator is linked immediately to grid-side.

Depending on the conventional vector control strategy, a robust control called Hinfinty (H∞) approach is designed and the problem of minimization has been derived by the standard minimization problem of mixed sensitivity.

Also, here, the mathematical representation of DFIG has been derived in suitable d-q reference frames. Th proposed method is utilized to control the active and reactive powers with the help of a conventional PI controller based on a VC strategy.

The work in [23] is to investigate the performance evaluations of DFIG based on CVDPC strategy. This control is applied for the RSC of DFIG. The analysis of symmetrical 3-phase ground fault and a single line-to-ground fault is presented. The results illustrate that the wind power conversion model can ordinarily work in the conditions of fault.

In other hand, numerous researches have been applied to achieve the wind turbine control processes in a wide range, such as fuzzy logic [25], [26], robust [27], optimal [28], [29] and adaptive controls [30], [31]. Although many advanced control techniques have been introduced for wind turbine controls, the PID mechanism is classified as the most suitable method in practices of engineering with some developments, e.g. [32], [33], [34]. The main reasons are the concept simplicity and easiness in design of structure of PID control.

Various methods have been applied due to pitch actuator fault accommodation, like, Kalman filtering [35], proportional multi-integral (PMI) observers [36], fuzzy Takagi-Sugeno control [37], and adaptive sliding mode fault tolerant control [32], [38].

Within these related researches [35], [39], [40], the control of fault-tolerant approach has divided into two essential points, detection of fault and accommodation of fault. In the detection of fault point, to estimate the fault accurately, the need of the size, type, location, and moment of the fault are presented. These data are then utilized in accommodation of fault part to overcome effects of fault. Furthermore, recently, a new mechanism has been introduced, where, as a part of the designed controller, the fault is estimated adaptively

[32], [38], [41]-[43]. The performance of this controller is critical to parameters of the design due to the accommodation and estimation of the fault being conducted simultaneously [32]. Although PID controller has a huge interest in designing the control of wind turbines, there are some considerable limitation points for PID controllers of such systems. First, a painstaking and ad-hoc process is needed in order to estimate the gains of PID. In order to determine PID gains, an ad-hoc and painstaking process is required. But, regardless of the existence of several techniques for tuning gains of PID [26], [34], [44], there exist no systematical method for the control process of wind turbine that estimates such gains which guarantees the performance and stability of the system.

Second, the effectiveness of PID controllers mostly appears on linearized wind turbines, and not for the whole behavior of nonlinear wind turbines. This point leads to design controllers depending upon the linearized models, assuming that the wind turbines are working at their optimal operational points. Hence, the obtained controller which has been constructed for the linearized model of wind turbine, would most likely not yield the desired performances on the nonlinear models [45].

Wherefore, the problem of long-lasting of PID control designing for wind turbine nonlinear approaches has been solved [46]. This work includes gains determination automatically and analytically while reaching the stability. As, the proposed controller has uses the common PID design, it needs lower computational cost, in addition to its simple structure.

By the way, unlike methods mentioned previously like parameter varying controller [33] and scheduling of the gain [47] that need linearizing process around many operational points, the proposed controller is capable of managing the entire behavior of nonlinear

dynamic of wind turbine systems. Additionally, the Lyapunov-based algorithm is used to design and determine the PID controller gains properly to produce acceptable performance for applications of industrial processes. likewise, compared to the previous researches such as fuzzy-logic that depends mostly on skills of designer, e.g., in defining rules of fuzzy [26], [34], the work introduces an analytically systematic concept for self-tuning the gains of PID control.

Recently, a huge attention has been directed to an optimization algorithm called artificial bee colony (ABC) for solving problems of optimization because of its search capability of population, robustness, implementation simplicity, and speed of convergence, [48]-[51]. Due to the aforementioned merits, the ABC is used in the optimization process of microgrid MG operations in terms of scheduling of resource generation, economic power dispatch, and performance [52] and several publications that applied ABC recently are [53]-[59]. Moreover, the ABC technique is characterized by its simplicity, robustness, and population-based stochastic optimization algorithm. Also, for tuning operation, it needs lower control parameters [63]-[66].

The work in [60] uses the artificial bee colony ABC algorithm in order to reduce the overall annual system cost. Whereas [61] models and manages a microgrid connected system using improved ABC technique. The object of this optimization was to minimize factors of emission, fuel cost, maintenance and operating cost. A multi-period ABC algorithm is proposed in [62] to provide economic dispatch, taking into account, storages, generations, and responsive load offers.

CHAPTER 3

METHODOLOGY

3.1 Similarities Between DPC and VC

This part shows the similarities between the DPC and VC mathematically to illustrate that these two strategies have some common basis [24].

3.1.1 Vector Control VC

Vector control VC is the widespread technique handled in DFIG based wind turbines. The control process of the stator active and reactive power is handled via the rotor current vector. This vector is decoupled into the stator power components through a synchronous reference frame. This process provides decoupling of the control process of active power from the reactive power.

The MPPT method is applied to determine the references of the stator active and reactive power and the requirements of the grid, respectively. Also, the stator flux-oriented frames (SFOF) are applied to provide the controller synchronization via the phase angle of the stator flux space vector. Hence, VC performance is extremely dependent on the stator flux position estimation. This could be a serious issue under the varying parameters of the machine or disfigured conditions of the voltage supplying. Wherefore, the stator voltage-oriented frame (SVOF) is applied to overcome this issue for the synchronization of the controller.

A phase locked- loop (PLL) design is applied to get the signal of controller synchronization from the stator voltage signal, see figure 3.1.

The active and reactive power of the stator are formulated as [2]

$$P_s = \frac{3}{2} Re(V_s i_s *) = \frac{3}{2}(V_{ds}i_{ds} + V_{qs}i_{qs}) \tag{1}$$

$$Q_s = \frac{3}{2} Im(V_s i_s *) = \frac{3}{2}(V_{qs}i_{ds} - V_{ds}i_{qs}) \tag{2}$$

V_{qs} is vanished as the stator voltage-oriented frame (SVOF) is utilized for the synchronizations of the controller and the simplified equations of stator power will be expressed as

$$P_s = \frac{3}{2} V_{ds}i_{ds} \tag{3}$$

$$Q_s = \frac{-3}{2} V_{ds}i_{qs} \tag{4}$$

Depending on the stator flux equations through a synchronous frame [6], the stator currents are expressed as

$$i_{ds} = \frac{-L_m}{L_s} i_{dr} \tag{5}$$

$$i_{qs} = \frac{-L_m}{L_s}\left(i_{qr} + \frac{V_{ds}}{w_s L_m}\right) \tag{6}$$

Substituting equations (5) and (6) into equations (3) and (4) gives

$$P_s = \frac{-3L_m}{2L_s} V_{ds} i_{dr} \tag{7}$$

$$Q_s = \frac{3L_m}{2L_s} V_{ds} \left(i_{qr} + \frac{V_{ds}}{w_s L_m} \right) \tag{8}$$

Therefore, the i_{dr} and i_{qr} currents are used, respectively, to control the stator powers.

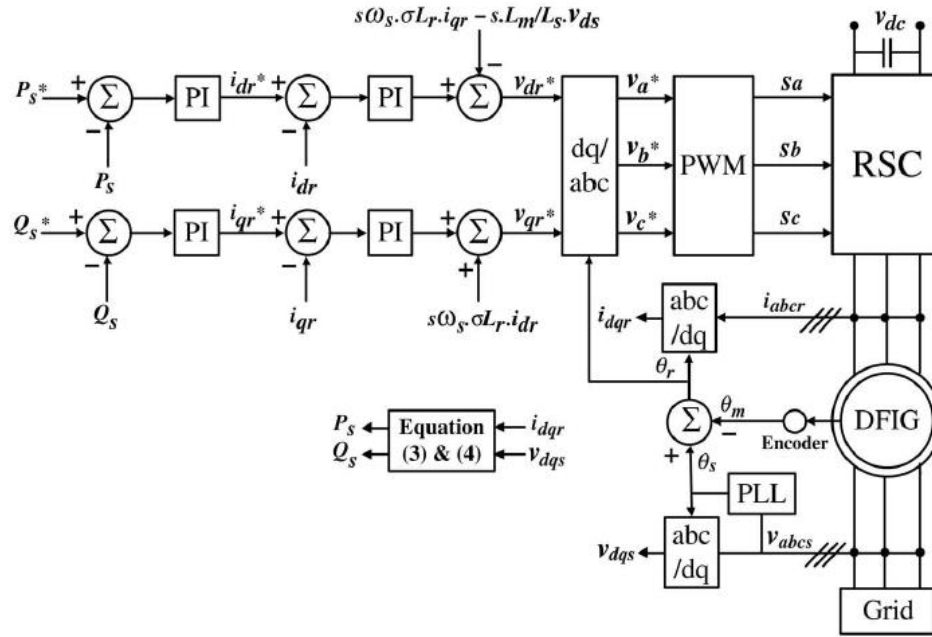Figure 3.1 shows the scheme of VC RSC-based.

Figure 3.1 Vector control VC block diagram [24]

3.1.2 Direct Power Control DPC

The principle of this strategy is to control the active and reactive power of stator and eliminate the current control loops. The DPC principles can be represented by the next two equations of the stator power [6]

15

$$P_s = \frac{-3L_m\omega_s}{2\sigma L_s L_r}|\varphi_s||\varphi_r|sin\delta \tag{9}$$

$$Q_s = \frac{3\omega_s}{2\sigma L_s}|\varphi_s|\left[|\varphi_s| - \frac{L_m}{L_r}|\varphi_r|\cos\delta\right] \tag{10}$$

By assuming that the stator and rotor flux have a constant magnitude, the next equation represents the derivative of equation (9) approximately,

$$\frac{dP_s}{dt} = \frac{-3L_m\omega_s}{2\sigma L_s L_r}|\varphi_s||\varphi_r|\frac{d\delta}{dt}\cos\delta \tag{11}$$

The equation (11) illustrates that the dynamics of stator active power are depending on the angle between rotor and stator fluxes (δ) variation. Thus, a rapid change in δ supplies a fast control for active power.

In the same vein, assuming that the stator flux and δ have a constant magnitude, the following equation represents the derivative of equation (10) approximately,

$$\frac{dQ_s}{dt} = \frac{-3L_m\omega_s}{2\sigma L_s L_r}|\varphi_s|\frac{d|\varphi_r|}{dt}\cos\delta \tag{12}$$

The equation (12) illustrates that the dynamics of stator active power are depending on the variations of the rotor flux magnitude. So, a rapid change in rotor flux magnitude provides a fast-reactive power control. Figure 3.2 shows the scheme of DPC RSC-based.
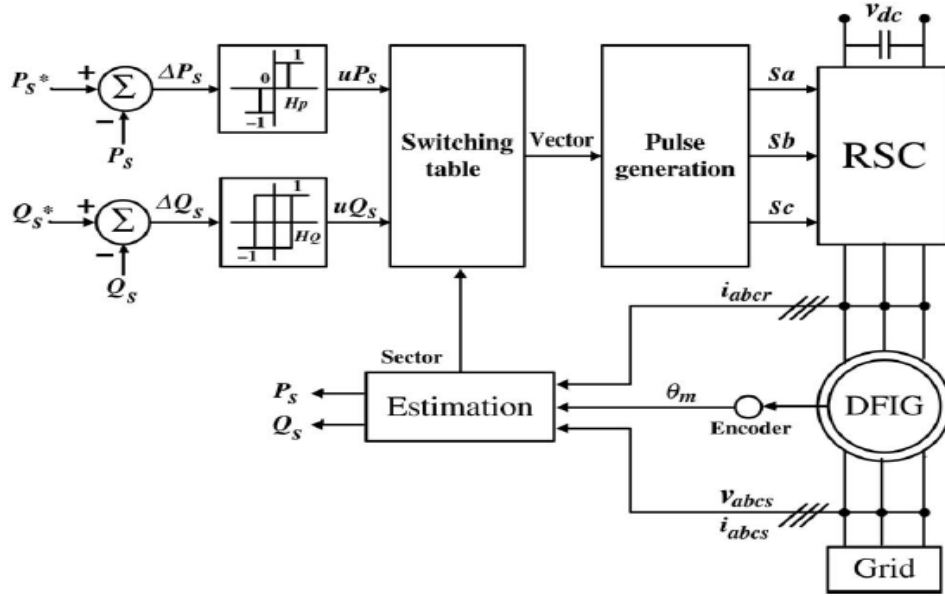
Figure 3.2 Direct power control DPC block diagram [24]

3.1.3 Mathematical Similarity Between VC and DPC

This sub-section shows the similarity between direct power control DPC and vector control VC mathematically to illustrate that these two strategies have some common basis.

In the vector control VC, by assuming a constant voltage for stator, the equations (7) and (8) show that

$$
\begin{cases}
P_s = \dfrac{-3L_m}{2L_s} V_{ds} i_{dr} \\
Q_s = \dfrac{3L_m}{2L_s} V_{ds} \left(i_{qr} + \dfrac{V_{ds}}{\omega_s L_m} \right)
\end{cases}
\Rightarrow
\begin{cases}
\Delta P_s \quad \alpha \quad -\Delta i_{dr} \\
\Delta Q_s \quad \alpha \quad \Delta i_{qr}
\end{cases}
\quad (13)
$$

Furthermore, taking into account the direct power control DPC principles, figure 3.3 represents the flux vector rotation of the rotor φ_r to φ_{r1} in a switching period of inverter. Here, φ_r is separated into its tangential components $\Delta\varphi_T$ and its radial components $\Delta\varphi_F$.

17

Depending on figure 3.3 and equations (9) and (10), the variations of the stator powers are written as

$$\Delta P_s = -K_1|\varphi_s|[|\varphi_{r1}|\sin(\delta + \Delta\delta) - |\varphi_r|\sin\delta] \qquad (14)$$

$$\Delta Q_s = -K_2 K_3|\varphi_s|\cos\delta[|\varphi_{r1}| - |\varphi_r|] \qquad (15)$$

Where K1, K2, and K3 are constant values and presented in [24]. Considering the small value of $\Delta\delta$, with a suitable $\cos\Delta\delta = 1$ approximation

$$\sin(\delta + \Delta\delta) = \sin\delta + \cos\delta . \sin\Delta\delta \qquad (16)$$

and

$$\sin\Delta\delta = \frac{\Delta\varphi_T}{|\varphi_r|} \qquad (17)$$

$$|\varphi_{r1}| = |\varphi_r| + \Delta\varphi_F \qquad (18)$$

Substituting equations (16) – (18) into equations (14) and (15) gives

$$\Delta P_s = -K_1|\varphi_s|\left[\Delta\varphi_T\cos\delta + \Delta\varphi_F\sin\delta + \frac{\Delta\varphi_T\Delta\varphi_F}{|\varphi_r|}\cos\delta\right] \qquad (19)$$

$$\Delta Q_s = -K_2 K_3|\varphi_s|\Delta\varphi_F\cos\delta \qquad (20)$$

The second term in equation (19) inside brackets has appeared because of the limited voltage vectors of inverter and failure of the inverter to decompose the tangential and radial flux components. The aforementioned term becomes highly small and virtually negligible by reducing the hysteresis controller bandwidth.
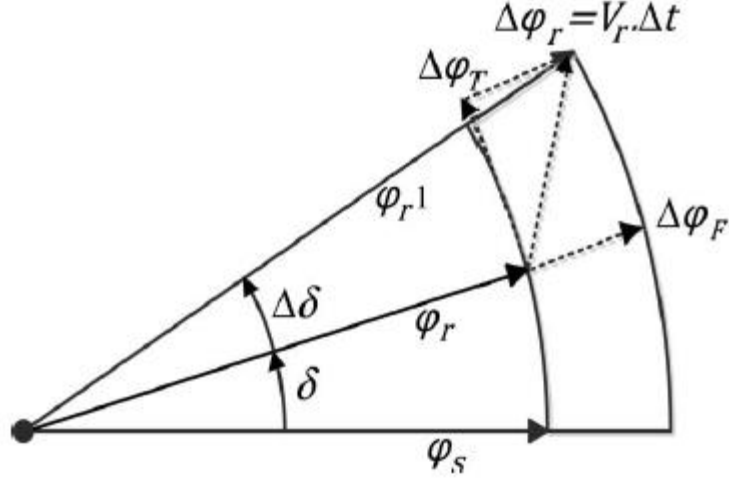
Figure 3.3 Variation of Flux linkage vector within a switching period in DPC [24]

Moreover, the third term inside the brackets consists of small terms multiplication, so, an appropriate approximation of the stator active powers variation is given as

$$\Delta P_s = -K_1 |\varphi_s| \Delta\varphi_T \cos\delta \qquad (21)$$

So,

$$\Delta P_s \quad \alpha \quad -\Delta\varphi_T \qquad (22)$$
$$\Delta Q_s \quad \alpha \quad -\Delta\varphi_F \qquad (23)$$

The equations (22) and (23) show that, the variation of the stator powers is negatively proportional to the radial and tangential component variations in the rotor flux. Comparing equation (13) with equations (22) and (23), the next results are gained

$$\Delta\varphi_T \quad \alpha \quad i_{dr} \qquad (24)$$

$$\Delta\varphi_F \quad \alpha \quad -i_{qr} \qquad (25)$$

i.e. The tangential and radial component variations of the rotor flux in direct power control DPC are act proportionally to the dq-axis components variation of the current vector of the

19

rotor in VC, respectively. Thus, there is a clear relationship between direct power control DPC and vector control VC strategies. Therefore, the CVDPC system can be modelled by,

$$P_s = -BV_{ds}i_{dr} \qquad (26)$$

Where $(\Delta P_s \quad \alpha \quad -\Delta i_{dr})$ & $(\Delta \varphi_T \quad \alpha \quad i_{dr})$

$$Q_s = BV_{ds}\left(i_{qr} + \frac{V_{ds}}{C}\right) \qquad (27)$$

Where $(\Delta Q_s \quad \alpha \quad \Delta i_{qr})$ & $(\Delta \varphi_F \quad \alpha \quad -i_{qr})$

and,

$$B = \frac{3L_m}{2L_s} \text{ and } C = \omega_s L_m$$

3.2   Artificial Bee Colony Optimization Algorithm ABC

In the proposed work of thesis, the ABC optimization algorithm is utilized to estimate the optimum value of the conventional PID controller coefficients used in CVDPC.

In (2005) Karaboga has discovered the Artificial Bee Colony ABC Optimization algorithm [41]. The mechanism depends on a search algorithm called swarm-based technique which is inspired by the behavior of a honey bee swarm foraging operation.

The goal of the process is to achieve the balance between optimal solutions during both local and global cases for a short computational time. Therefore, ABC is a highly efficient optimization mechanism and strong in dealing with huge and complicate stability conditions, such as the power systems stability that have high complexity and changing designs.

Furthermore, ABC algorithm enjoys several benefits, like structure flexibility, lower

computational time, robustness, simple tuning and implementation; these advantages make it appropriate for practical complicated power systems [67].

The forage selection of ABC algorithm has three main components:

1. Food Sources: the probable solutions for the optimized process. Their quality values depend on several branches, such as energy richness of the food source, the nest distance from the food source to the nest and the simplicity rate of energy extracting.

2. Employed bees: it is the group of bees that are related with a certain food source which is presently exploiting. This group shares the information related to the source with onlooker bees with a specific probability, which contains the source profitability, the nest distance and direction from the source.

3. Unemployed bees: this group of bees has to wait for the information from the employed bees. This type of bees is classified into two sorts of unemployed bees: scouts, whose task is to search for new food sources around the nest, and onlooker bees, which have to wait in the nest to take choice for the source depending on the information received from the employed bees.

3.2.1   Initial Population

In the initial stage, ABC algorithm randomly produces SN number of D-dimensional vectors, where SN refers to the number of food sources. The following vector is considered as the ith food source inside the population $X_i = (x_{i,1}, x_{i,2}, \ldots, x_{i,n})$. So, initial food source is produced by:

$$x_{i,j} = x_j{}^{min} + rand(0,1)\left(x_j{}^{max} - x_j{}^{min}\right) \tag{28}$$

$$i = 1,2,3, \dots, n \qquad j = 1,2,3, \dots, D$$

Where D is the parameter number of optimizations. $x_j{}^{min}$ and $x_j{}^{max}$ are lower bound and upper bound for parameter j. After the population has been initialized, the iterative search operations are applied over the employed, onlooker and scout bees as below:

3.2.2 Employed Bee Phase

A new candidate solution V_i is generated by every employed bee X_i around its present position. The new solution position is presented as:

$$v_{i,j} = x_{i,j} + \emptyset_{i,j}\left(x_{i,j} - x_{k,j}\right) \tag{29}$$

Where $k = 1,2,3, \dots, SN$ and $j = 1,2,3, \dots, D$ are random indexes, k must be different from i. $\emptyset_{i,j}$ is a random number in the period [−1, 1].

If the values of parameter generated by equation (29) exceed the limits, the value will be replaced by the value's limit of the parameter. Therefore, fitness values are determined for the candidate solution V_i. But, if this fitness value of V_i is greater or equal then the fitness value of X_i,the value of X_i will be updated by the new candidate solution (V_i), otherwise X_i is kept the same.

3.2.3 Probability of Onlooker Bee

As the employed bee group completes the search task; all onlooker bees choose one food source depending on the probability of food source determined by the next formula:

$$P_i = \frac{fitness_i}{\sum_{n=1}^{SN} fitness_i} \qquad (30)$$

The probability of choosing a certain food source by the onlooker bees is bigger as the food

source's fitness is bigger.

3.2.4 Unemployed Bee Phase

After the onlooker bees select the appropriate food source X_i, onlooker bees apply some

adjustments on X_i utilizing equation (29). If the adjusted food source quality is better or at

least equal then the old one, X_i will be substituted by the adjusted food source.

If a food source X_i does not develop over a certain generation number called limit L, a new

food source is replaced over the current food source. This new food source is founded by

the scout bee. The new source is generated by scout by handling the following formula:

$$x_{i,j} = x_j{}^{max} + rand(0,1)\left(x_j{}^{max} - x_j{}^{min}\right) \qquad (31)$$

3.2.5 Objective Function

In the proposed work, the ABC optimization algorithm is used to determine the optimum

value of the coefficients of PID controller.

The integral of the squared error (ISE) of the stator output power is formulated as an

objective function to optimize the conventional PID controller coefficients.

The ISE based cost function for the test power system is represented by:

$$J = \int_0^{T_{sim}} (\Delta\omega_i(t))^2 . dt \tag{32}$$

And the parameters are subjected to these constraints:

$$\left.\begin{array}{c} K_p{}^{min} \leq K_p \leq K_p{}^{max} \\ K_i{}^{min} \leq K_i \leq K_i{}^{max} \\ K_d{}^{min} \leq K_d \leq K_d{}^{max} \end{array}\right\} \tag{33}$$

Where i is the i_{th} generator and T_{sim} is the simulation time.

The scheme of the coefficients of the conventional PID controller is shown in Figure 3.4 where the ABC algorithm is used to minimize the error between the rotor output current and its reference to obtain the optimal set of conventional PID controller coefficients.
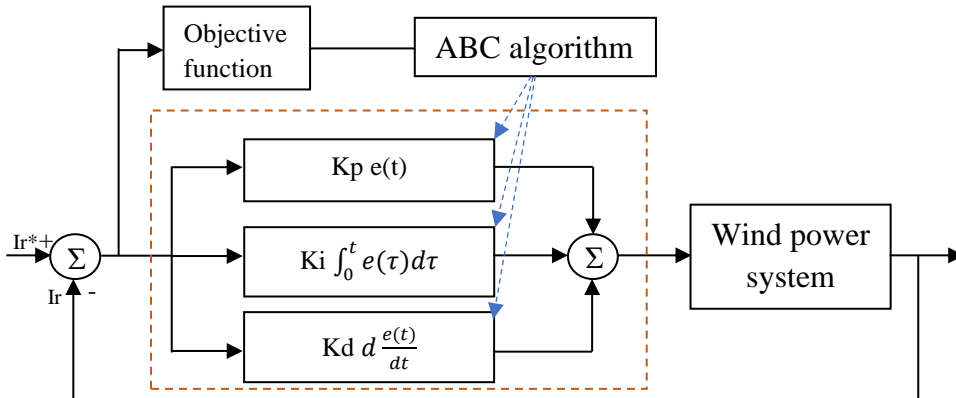

Figure 3. 4 Conventional PID controller coefficients tuning scheme using ABC Algorithm
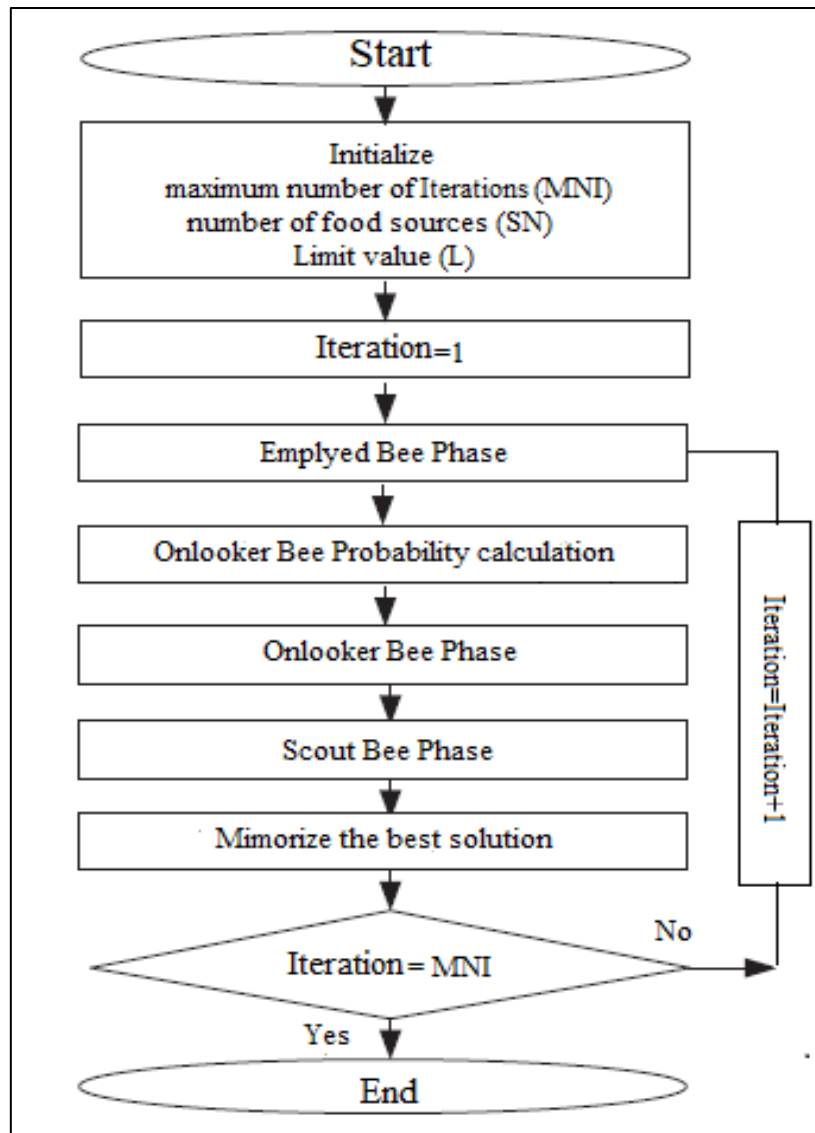
Figure 3.5 ABC Algorithm Flowchart

The scaling factors scheme of the CVDPC-conventional PID based is shown in figure 3.5 where the ABC algorithm is handled to estimate the gains of PID controller coefficients and then used to run the system to get best results as possible.

3.3 The Proposed PID Adaptive Controller

3.3.1 Conventional PID

The main advantage of conventional PID controller is its ability to handle the three control terms of proportional, integral and derivative effect on the output of controller to get suitable and optimal control. Figure 3.6 illustrates how the controller is connected and applied to the system in the case of conventional PI-based and conventional PID-based controllers. It shows that the input of the PID controller is the error between the actual rotor current (I_{dr}, I_{qr}) and its reference ($I_{dr}*$, $I_{qr}*$), while its output is the controlled signal (U_{co}) that controls the stator power of the system. In the proposed approach, the PID controller coefficients are fixed.
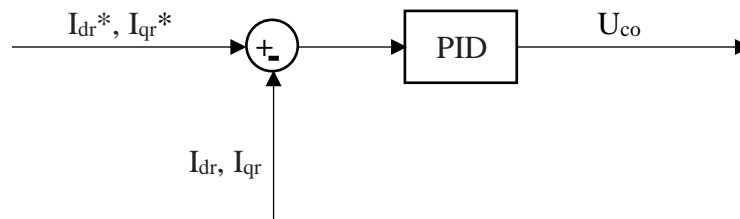

Figure 3.6 Conventional PID connection

This conventional PID strategy is applied in the first two objectives of the work, which are CVDPC conventional PI-based and CVDPC conventional PID-based.

3.3.2 Adaptive PID Controller

In order to achieve the proposed CVDPC adaptive PID-based controller, two techniques are used to estimate the PID controller coefficients adaptively, model reference adaptive control MRAC and least square method LSM.

The model-reference adaptive control MRAC is used to enhance the performance of the system control signal and estimate the values of the PID controller coefficients adaptively. The MRAC model consists of three essential components, reference model signal, control signal and adaptive part.

The proposed controller has a simple feedback loop known as inner loop composed of the PID controller signal u_{PID} and the process of MRAC and another feedback loop called outer loop attached to the adaptive mechanism that estimates and updates the PID controller coefficients adaptively as shown in figure 3.7.
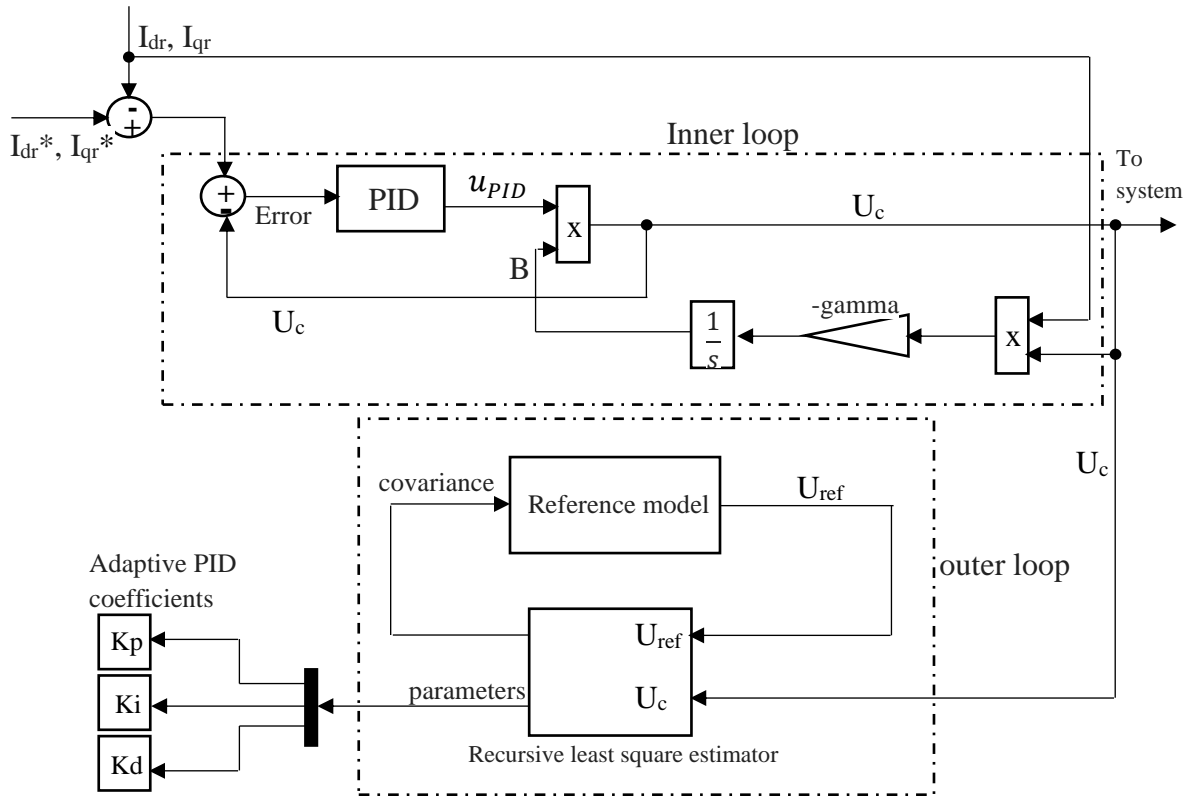

Figure 3. 7 The proposed adaptive PID controller diagram using MRAC technique

The mechanism for estimating the PID coefficients in a model reference adaptive system can be achieved by using a least square method LSM. This process uses reference model

signal U_{ref} and controller output signal U_c to estimate the PID controller coefficients (Kp, Ki, and Kd).

As can be seen, the adaptive part represented by the least square method which depends on the controller output signal U_c and the reference model transfer function output, Whereas the output is the new estimated values of the PID coefficients.

The reference model signal tells about how the system output must respond optimally to the optimal reference signal. The reference model transfer function that used in this work gives approximately no overshoot and its settling time is nearly similar to that of the proposed system, as shown in figures 3.8.
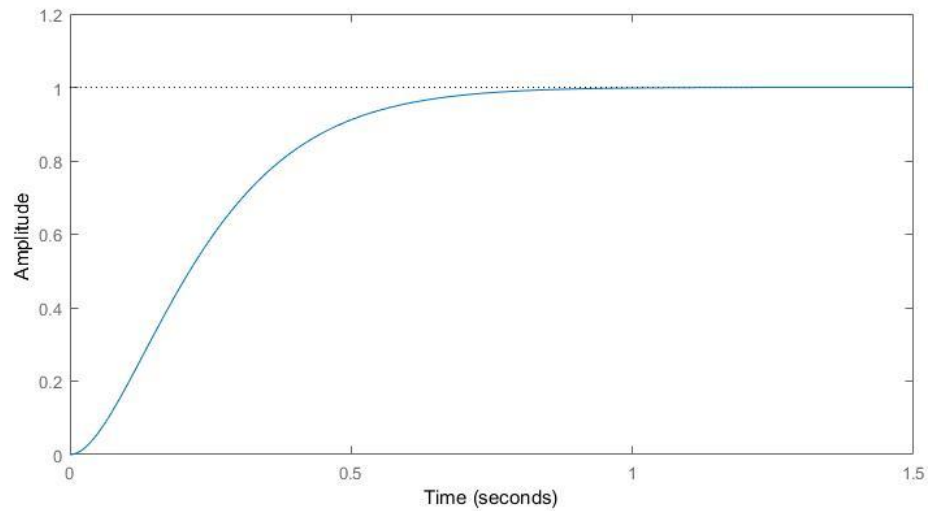

Figure 3.8 Ideal reference model signal of MRAC controller

Figure 3.8 shows the ideal case of the reference model transfer function output U_{ref}.

The controller uses a fixed adaption gain called $gamma$, where $gamma$ is a positive quantity that indicates the controller adaptation gain. $Gamma$ is a scaling factor which is used to scale the output signal of the proposed adaptive controller.

For larger values of $gamma$, system responses quickly with high overshoots, and for smaller values of $gamma$ system responses slowly with small overshoots. So, usually $gamma$ is chosen as small as possible and in this work, $gamma$ chosen to be 0.2 by trial and error, see figure 3.10.
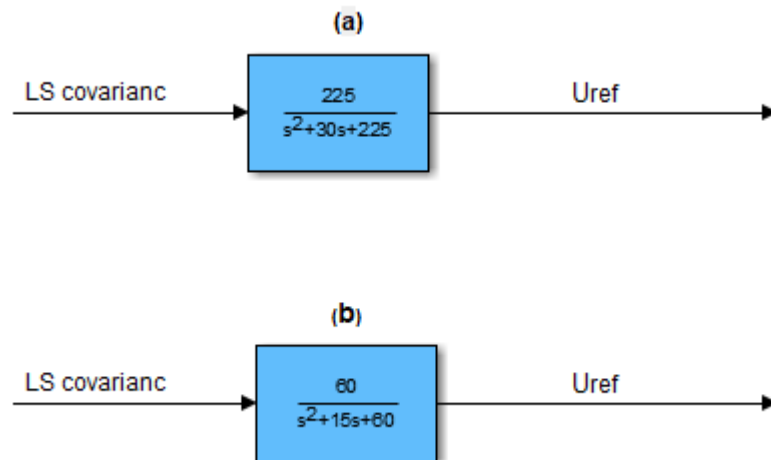
Figure 3.9 shows two different types of transfer function,

(a)

LS covarianc → $\dfrac{225}{s^2+30s+225}$ → Uref

(b)

LS covarianc → $\dfrac{60}{s^2+15s+60}$ → Uref
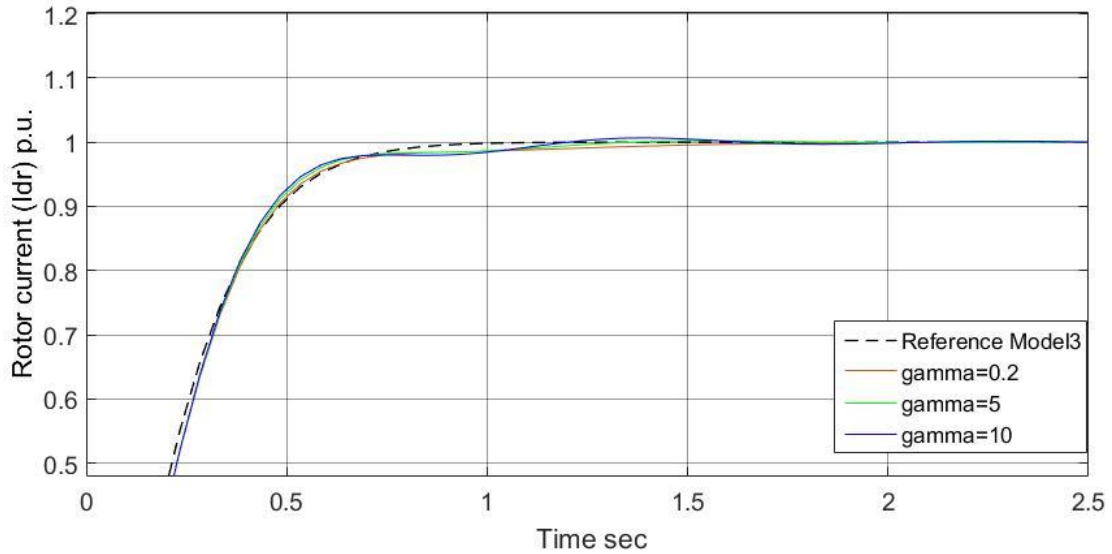
Figure 3.9 Two different types of transfer function

Figure 3.10 Rotor current I_{dr} in p.u. with gamma = 0.2, 5, and 10 during transfer function in figure 3.8 (a)

The reference signal part of the MRAC model is referred to the optimal magnitude of the closed loop system. i.e. how the system is desired to behave.

Selection of the reference model transfer function should be highly considered in order to have a matched raising time response between the transfer function and the desired output of the system and the amount of overshooting as well.

Figure 3.10 shows the system response for the transfer function in figure 3.9 (a), while figure 3.11 represents the response of the system when the transfer function in figure 3.9 (b) is applied.
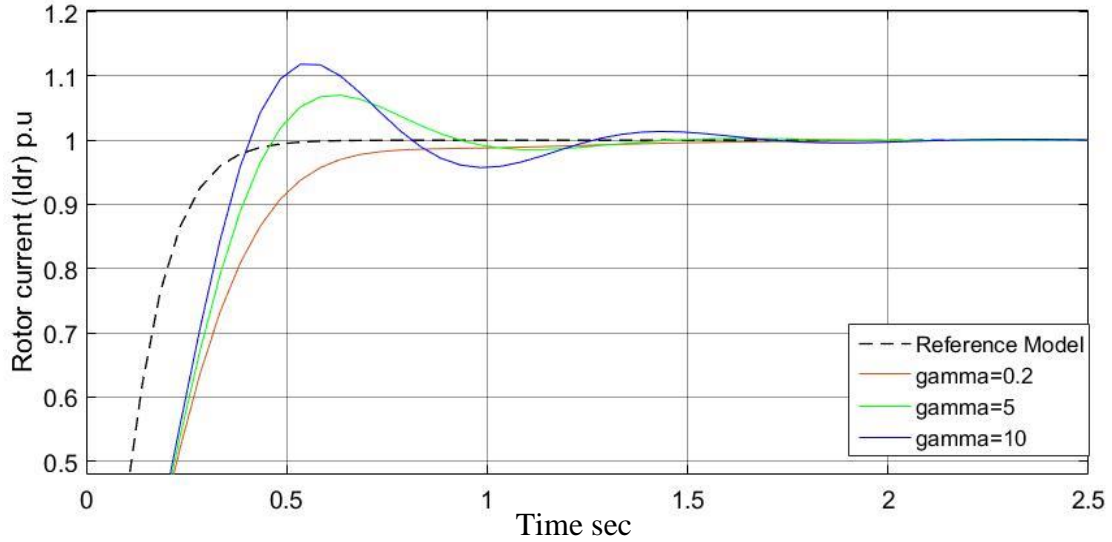
Figure 3.11 Rotor current Idr in p.u. with gamma = 0.2, 5, and 10 during transfer function in figure 3.8 (b)

Since, the raising time of the transfer function in figure 3.9 (a) and its overshoot is better than that of the transfer function in figure 3.9 (b), the transfer function in figure 3.9 (a) is chosen to be the model reference of the proposed adaptive controller.

The main goal of the reference model signal is to guide LSM to estimate the PID controller coefficients adaptively in order to make the output signal of the proposed controller controls the system as close as possible to the desired output U_{ref}.

The MRAC controller generates a signal B which used to scale and enhance the behavior of the PID controller output signal u_{PID} and make it appropriate and optimal to control the system.

$$\widehat{U}c = Uco * B \tag{34}$$

Where $\hat{U}c$ is the new controlled signal regarding to the new estimated PID coefficients ($\hat{K}$p, $\hat{K}$i and $\hat{K}$d).

$$\hat{u}_{PID}(t) = \hat{K}p\ e(t)\ +\ \hat{K}i\int_0^t e(\tau)d\tau + \hat{K}d\ \frac{d}{dt}e(t) \tag{35}$$

$$B = -gamma\int_0^t Idr\ Uc(t)dt \tag{36}$$

Moreover, the LSM approach is applied to estimate and update the PID controller coefficients (Kp, Ki and Kd) adaptively.

Figure 3.12 shows the block diagram of the recursive least square estimator, where, the reference model signal (U_{ref}) and (U_c) are considered as the input of the least square regressor while the output is the new estimated values of the PID controller coefficients (Kp, Ki and Kd).
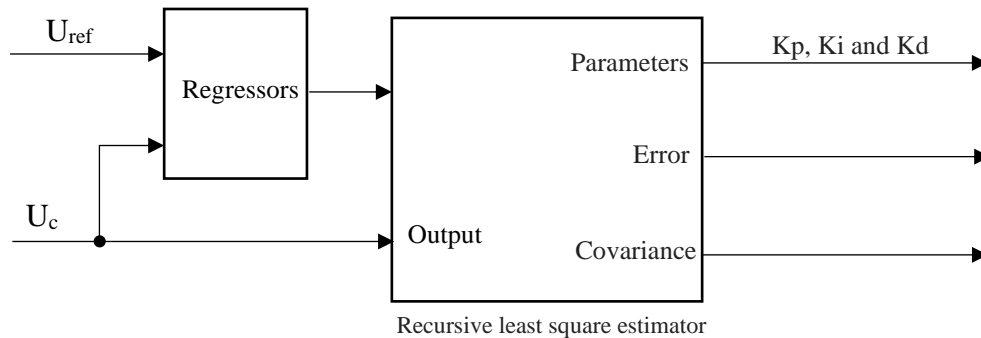

Recursive least square estimator

Figure 3.12 Recursive least square estimator diagram

The proposed adaptive controller block diagram is shown in figure 3.7. The diagram represents the components of the MRAC model and their connection. The input signal to the adaptive controller is the difference between the actual rotor current (I_{dr}) and its reference current (I_{dr}^*) whereas the output signal is the control signal (U_c) that is used to control the stator power P_s of the wind farm.

As mentioned before, the equation of conventional PID controller can be written as,

$$u_{PID}(t) = K_p e(t) + K_i \int_0^t e(\tau)d\tau + K_d \frac{d}{dt} e(t) \tag{37}$$

Considering $U_{PID}(\theta)$ is the PID controller transfer function and θ indicates the parameter vector (Kp, Ki, Kd) to be tuned [68], [69].

$$U_{PID}(s) = [K_p \quad K_i \quad K_d] \begin{bmatrix} 1 \\ \dfrac{1}{s} \\ \dfrac{s}{\tau s + 1} \end{bmatrix} \tag{38}$$

Where the derivative $\frac{d}{dt}$ transfer function is written approximately as, $\frac{s}{\tau s+1}$.

Then,

$$\theta^T = [K_p \quad K_i \quad K_d]$$

$$\emptyset_1 = \begin{bmatrix} 1 \\ \dfrac{1}{s} \\ \dfrac{s}{\tau s + 1} \end{bmatrix} \tag{39}$$

Hence, equation (38) can be formed as,

$$U_{PID}(s) = \theta^T \emptyset_1 \tag{40}$$

Mainly, the main objective of the proposed controller is to estimate and update the PID controller coefficients adaptively such that the transfer function of the closed loop is as close as possible to the reference model transfer function signal.

Now, we denote a discretize model of $\emptyset_1(s)$ by $\emptyset_1(z)$ and the PID controller will be,

$$U_{PID}(z, \theta) = \theta^T \emptyset_1(z) \tag{41}$$

According to the method of fictitious reference iterative tuning FRIT [69][70], a closed loop experiment is performed to get the data of input $u_{PID_0}(k)$ and output $U_{c_0}(k)$, $k = 1, ..., N$ for the initial controller coefficients Θ_0 and the reference signal $U_{ref}(k)$. So, the following equation calculates the fictitious reference signal,

$$\tilde{U}_{ref}(\Theta, k) = U_{PID}(z, \theta)^{-1} u_{PID_0}(k) + U_{c_0}(k) \tag{42}$$

Using this signal, the controller coefficients Θ are tuning and the following J is minimized,

$$J(\Theta) = \sum_{k=1}^{N} [U_{c_0}(k) - M(z)\tilde{U}_{ref}(\Theta, k)]^2 \tag{43}$$

Where M(s) is the given reference model transfer function.

To apply LSM, first, by assuming the ideal case of error [68],[69],

$$U_{c_0}(k) - M(z)\tilde{U}_{ref}(\Theta, k) = 0 \tag{44}$$

By substituting equation (42) into equation (44) and then multiplying both sides by $U_{PID}(z, \theta)$, we get,

$$U_{PID}(z, \theta)U_{c_0}(k) = M(z)u_{PID_0}(k) + U_{PID}(z, \theta)M(z)U_{c_0}(k) \tag{45}$$

In order to achieve the tuning process, the next relation is minimized,

$$\hat{J}(\Theta) = \sum_{k=1}^{N} \hat{\varepsilon}(k)^2 \tag{46}$$

Where,

$$\hat{\varepsilon}(k) = U_{PID}(z, \theta)(1 - M(z))U_{c_0}(k) - M(z)u_{PID_0}(k) \tag{47}$$

Although the controller coefficients tuning method is carried out online, sometimes the values of these coefficients are abruptly updated within a certain period of time, this may deteriorate the performance of the controller [69].

To solve this problem, the initial data $u_{PID_0}(k)$, $U_{c_0}(k)$ are replaced by $u_{PID}(k)$, $U_c(k)$ for equation (47), [69].

$$\emptyset(k) = \emptyset_1(z)\big(1 - M(z)\big)U_c(k) \tag{48}$$

$$d(k) = M(z)u_{PID}(k) \tag{49}$$

So, the error will be,

$$\hat{\mathcal{E}}(k) = \theta^T \emptyset(k) - d(k) \tag{50}$$

As the standard LSM uses all input, output data $u_{PID}(k)$, $U_c(k)$ from the initial time to the current time, sometimes the standard LSM cannot manage the plant characteristic variations. Therefore to overcome this issue, a forgetting factor ($0 < \lambda < 1$) is used with the LSM [69]. when $\lambda = 1$, the standard LSM is obtained.

The new performance index of LSM can be expressed as,

$$\hat{J}(\Theta) = \sum_{k=1}^{N} \lambda^{N-k}\hat{\mathcal{E}}(k)^2 \tag{51}$$

Least square algorithm is a method which estimates the optimal values of $\hat{\theta}(k)$ of the PID controller coefficients by using $\hat{\theta}(k-1)$. So, using equation (51), the new LSM equations will be as follows,

$$\hat{\theta}(k) = \hat{\theta}(k-1) + K(k)[u_{PID}(k) - \emptyset(k)^T\hat{\theta}(k-1)] \tag{52a}$$

$$K(k) = P(k-1)\emptyset(k) \, X \, [\lambda + \emptyset(k)^T P(k-1)\emptyset(k)]^{-1} \tag{52b}$$

$$P(k) = [P(k-1) - K(k)\, \emptyset(k)^T\, P(k-1)]/\lambda \qquad (52c)$$

Where P is the correlation matrix and K is adaptation gain. As a result, the PID controller coefficients $\hat{\theta}(k)$ will be updated recursively by using the above equations of LSM.

CHAPTER 4

SIMULATION RESULTS and DISCUSSION

Here, the MATLAB Simulink is used to simulate the system. The simulation is handled

using a 9-MW wind energy system. It consists of six wind turbines DFIG-based and every

one of them provides 1.5-MW. This model is used to study the performance of CVDPC

strategy by using conventional PI, conventional PID and adaptive PID controllers based.

Figure 4.1 demonstrates the graph of the model used in simulation and the parameters are

given in Table 4.1. Ordinarily, to achieve the proposed techniques, the simulation is divided

into two sections: first section concentrates on the steady-state condition and the second is

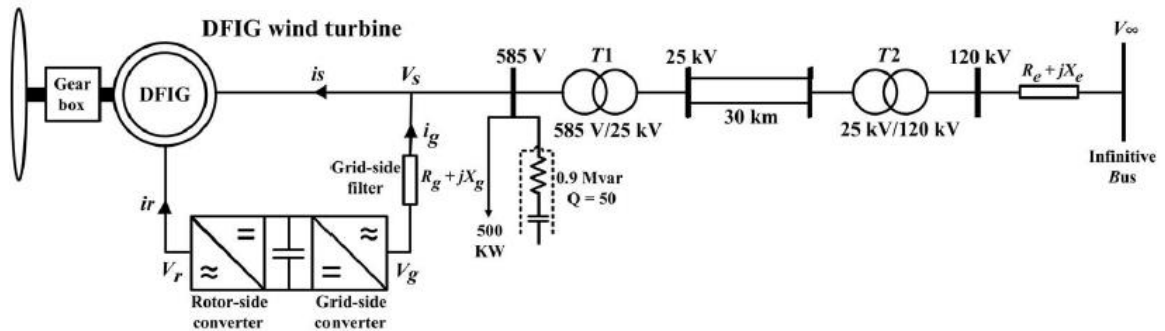related to the robustness issue against parameters variation.

Figure 4.1 The simulated system schematic diagram [24]

Table 4.1 Simulation parameters

Parameter	Value
V_{base}	575 V
R_s	0.023 p.u.
R_r	0.016 p.u.
L_s	0.18 p.u.
L_r	0.16 p.u.
L_m	2.9 p.u.
Nominal stator active power	7.58 MW
Nominal stator active power	1.42 MW
ω_r	1.2 p.u.
Conventional PI Kp, Ki	0.6, 8
Conventional PID Kp, Ki, Kd	9.5, 9, 0.1

4.1   Adaptive PID Controller Using Model Reference Adaptive Control MRAC

As mentioned before, the proposed adaptive controller is modeled and designed using a direct adaptive mechanism called model reference adaptive controller MRAC. The PID controller that is used in CVDPC controller of the wind farm system uses the MRAC to tune its values (Kp, Ki and Kd) adaptively, see figure 4.2. The MRAC model consists of three essential components, reference signal, control signal and adaptive part.
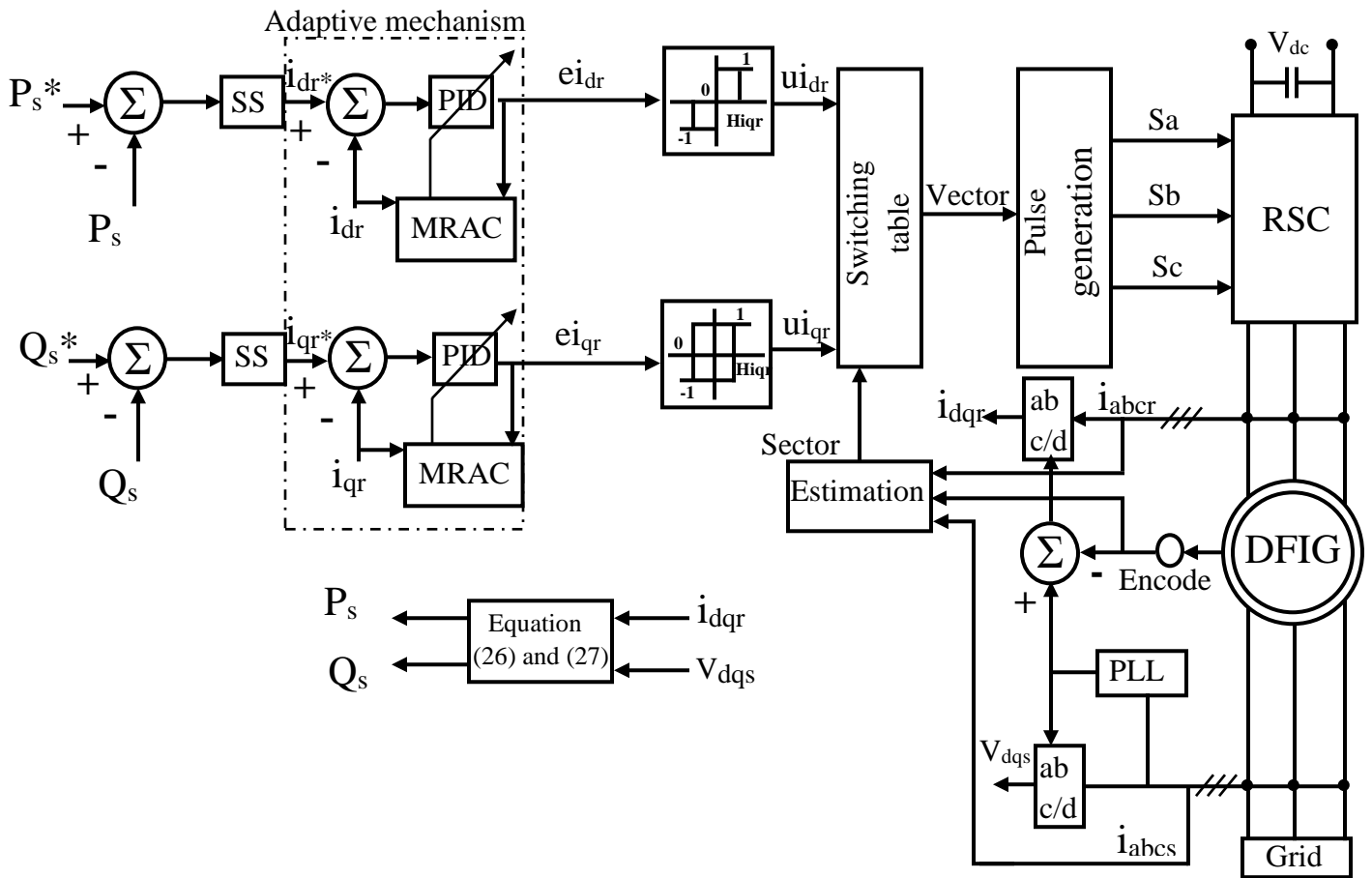
Figure 4.2 Adaptive PID controller structure

As seen, the input signal to the adaptive controller is the difference between the actual rotor

current (i_r) and its reference current (i_r*) and the output signal is the control signal (ei_r) that

is used to control stator power Ps of the wind farm.

4.2   Steady-State Condition

The next two sections illustrate the steady-state condition results of the system for   0 < t < 0.3 seconds. The wind speed is assumed to be 15 m/s when the generator rotates at $\omega_r = 1.2\ pu$. As a result, 9 MW is produced from the wind system. As the DFIG rotates at synchronous speed with slip $s = -0.2$, the system generates active powers ($P_s = 7.58\ MW$ and $P_r = 1.42\ MW$) which is supplied via both rotor and stator windings to the grid.

4.2.1   Steady-State Condition of CVDPC Conventional PI-based and Conventional PID-based with Identical PI coefficients

In this part, the values PI coefficients (Kp and Ki) in both methods have assumed to be similar and then, the comparison has been achieved.
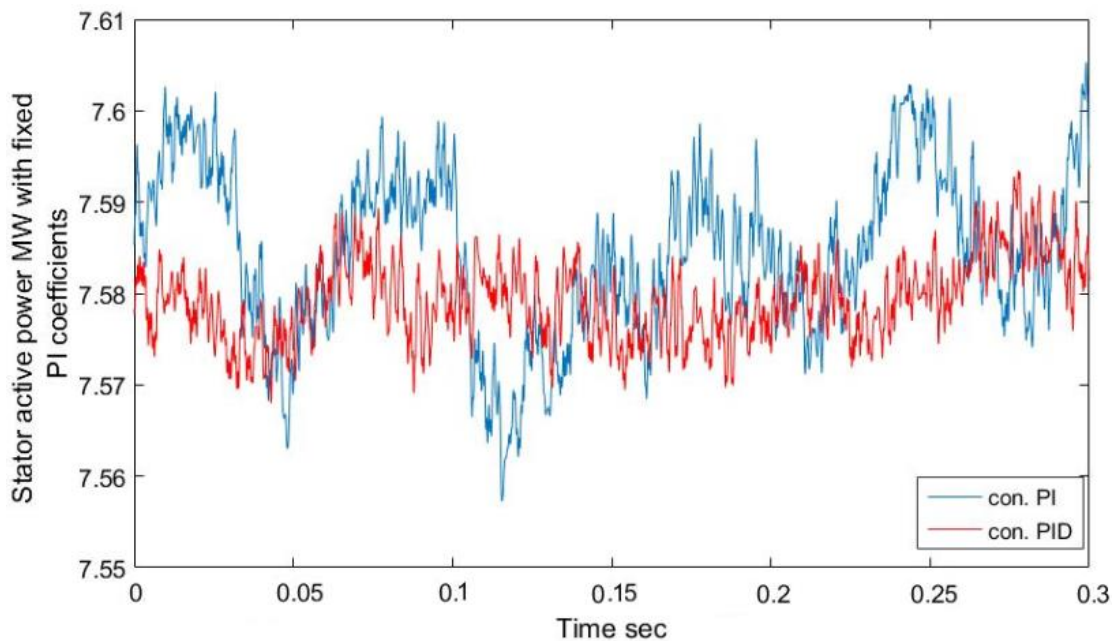

Figure 4.3 Stator active power with identical PI coefficients
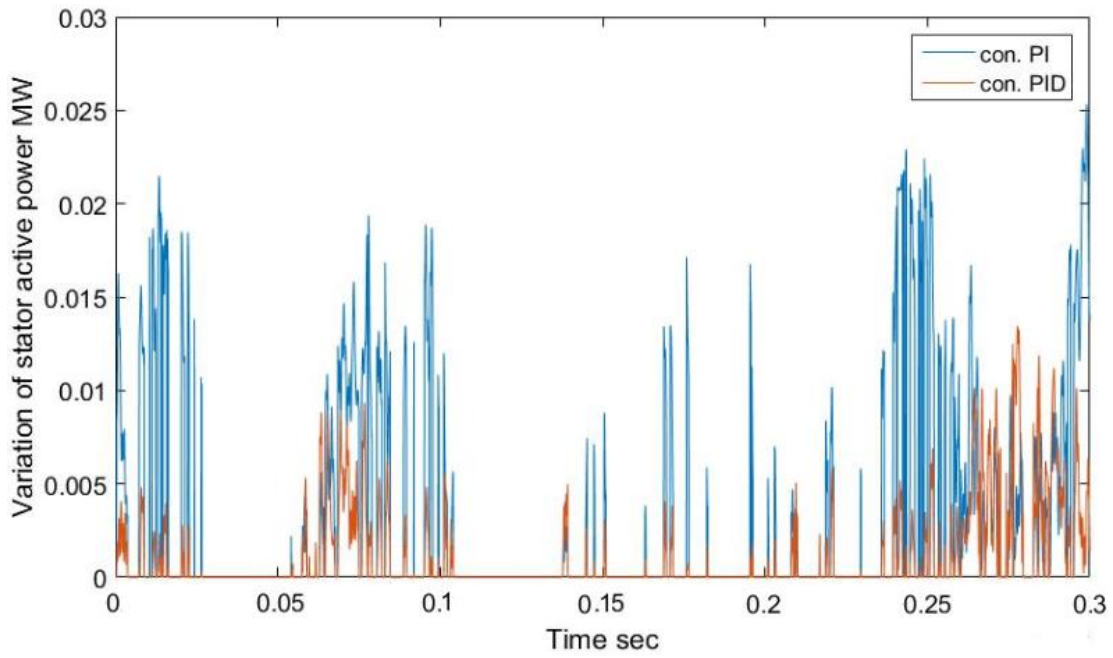
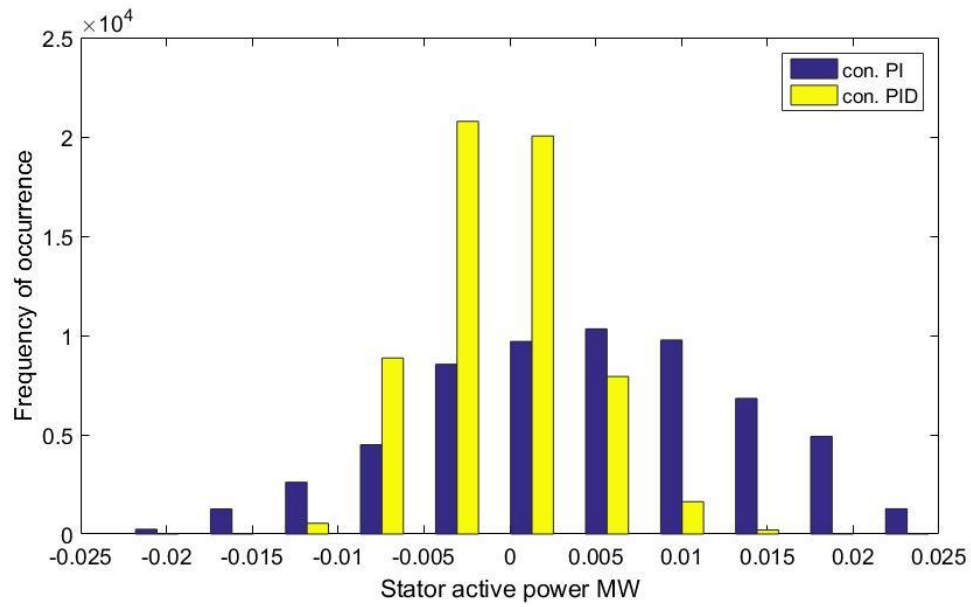Figure 4.4 Stator active power points above nominal value

Figure 4.5 Histogram of ramp rate for stator power (MW)

Table 4.2 Comparison of CVDPC- conventional PI-based and PID-based with identical PI coefficients

CVDPC	Stator side		Rotor side	
	MW	%	MW	%
PI-based	0.028	0.37%	0.015	1.01%
PID-based with identical PI coefficients	0.0135	0.16%	0.008	0.57%

As seen from figures 4.3 and 4.4, the maximum value that the stator has reached above the nominal value for the CVDPC- conventional PI controller-based is (0.028MW) which represents (0.37%) of the nominal value of the stator active power. On the other hand, the maximum value of stator active power for the CVDPC- conventional PID controller-based with similar values of Kp and Ki is (0.0135MW) which represents (0.16%) of the nominal value, see table 4.2.

Hence, the CVDPC- conventional PID controller-based gives a smaller fluctuation compared with that of CVDPC- conventional PI controller-based by (56.75%).
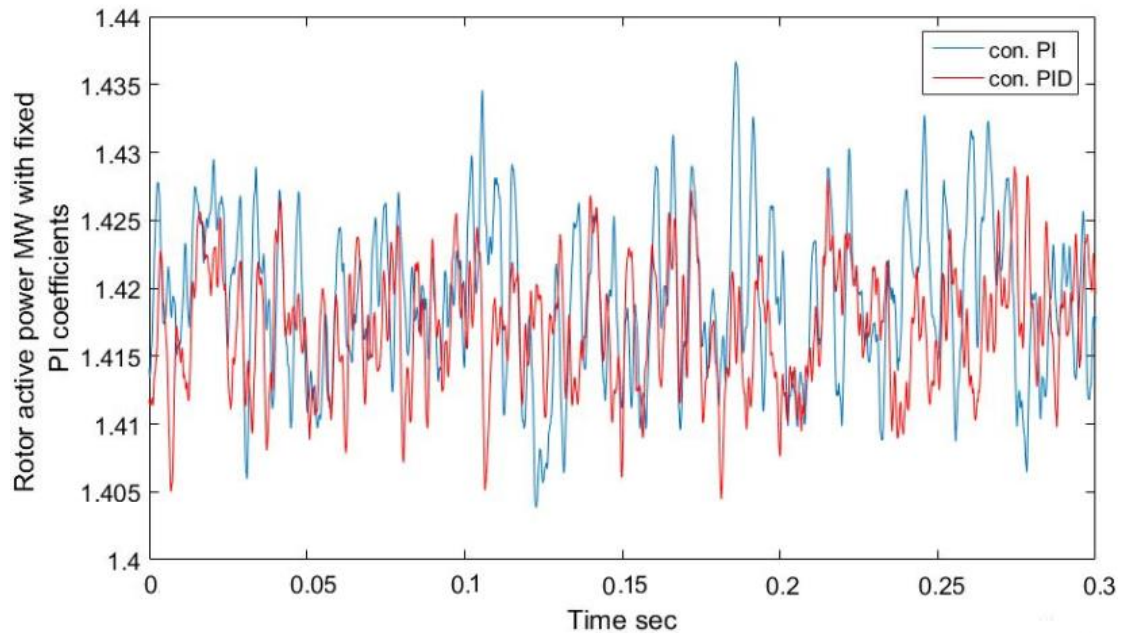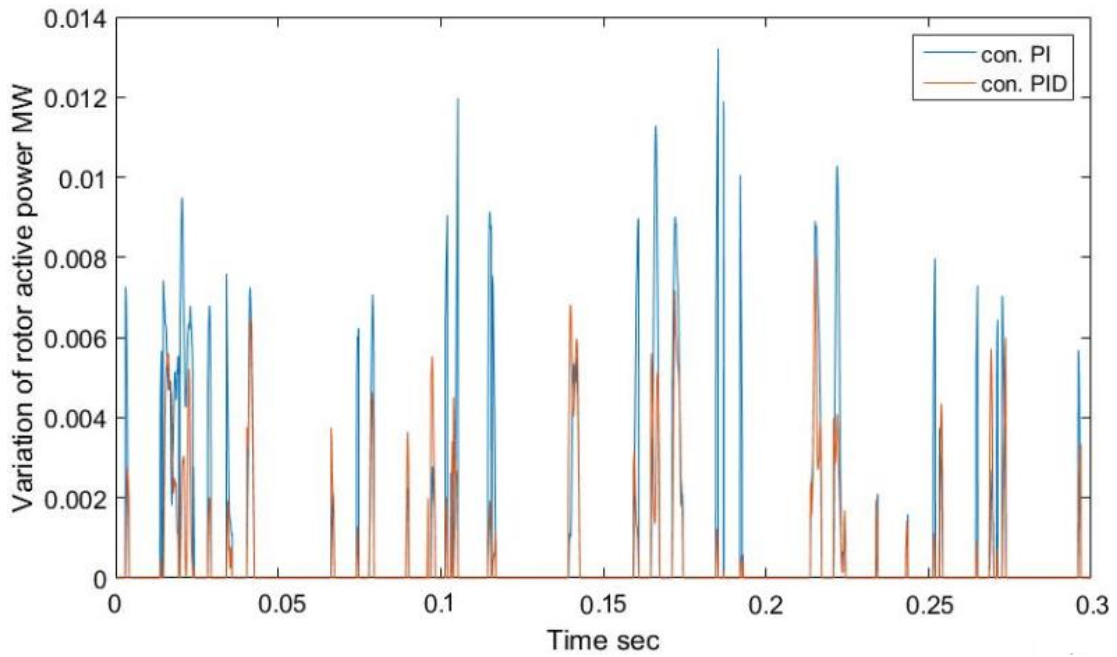
Figure 4.6 Rotor active power

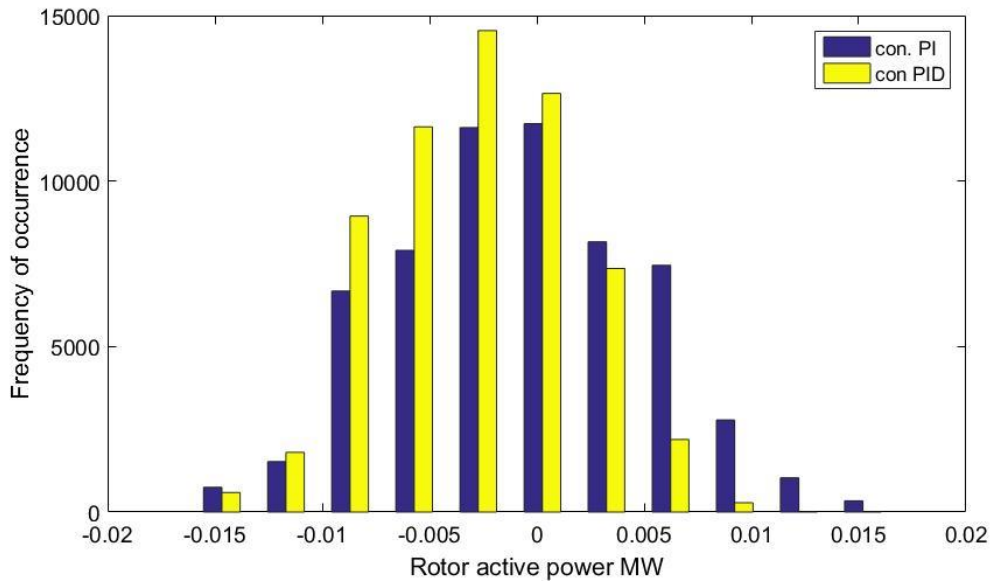Figure 4.7 Rotor active power points above nominal value

Figure 4.8 Histogram of ramp rate for rotor power (MW)

In the same manner, figures 4.6 and 4.7 show that the rotor active power reached (0.015MW) above the nominal value for CVDPC- conventional PI controller-based which represents (1.01%), and for CVDPC- conventional PID controller-based, it reached (0.008MW) of the nominal value which is (0.57%), see table 4.2 as well. So, in case of using identical values of Kp and Ki, the CVDPC- conventional PID controller-based gives a smaller fluctuation compared to that of CVDPC- conventional PI controller-based by (43.56%).

Figures 4.5 and 4.8 show the location of each active power points for the CVDPC- conventional PI controller-based and CVDPC- conventional PID controller-based with similar Kp and Ki values and their distance from the nominal value, respectively. The system with conventional PID-based controller has more active power points located around the nominal value than that of the system with conventional PI-based controller,

44

hence, the use of conventional PID-based controller is better than the use of conventional

PI-based when the values of Kp and Ki are assumed to be equal.

4.2.2 Steady-State Condition of CVDPC Conventional PI-based and Conventional PID-based with different values of PI coefficients

Here, the values of Kp and Ki of CVDPC- conventional PID controller-based are assumed

to be different than those of CVDPC- conventional PI controller-based and chosen

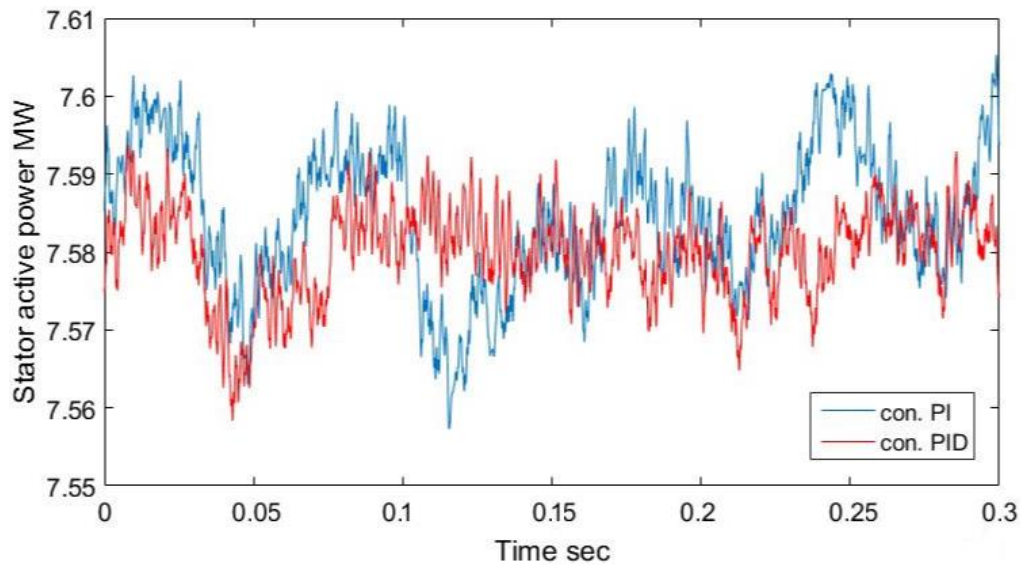carefully using an optimization method called the Artificial Bee Colony (ABC).

Figure 4.9 Stator active power with different values of Kp and Ki

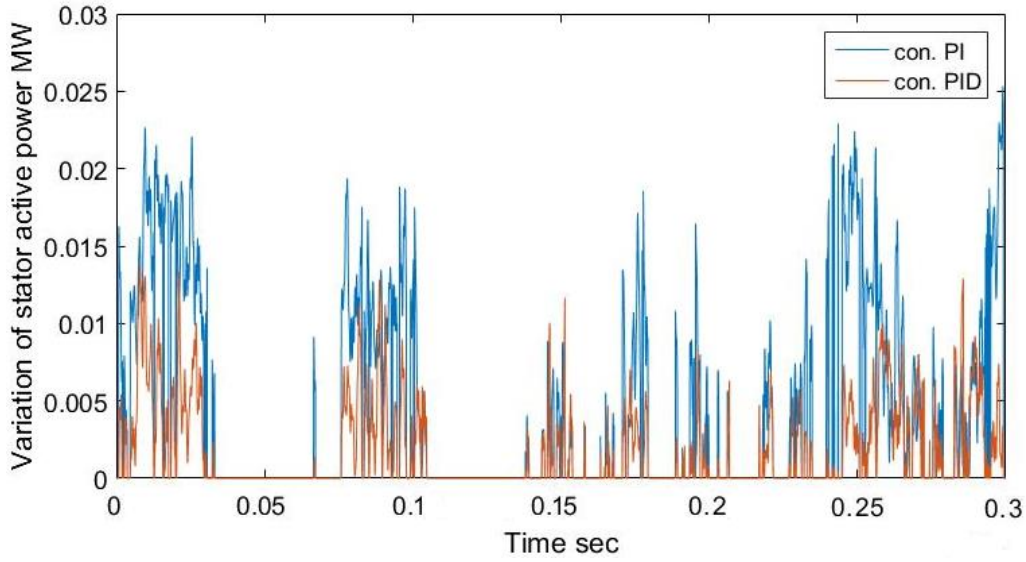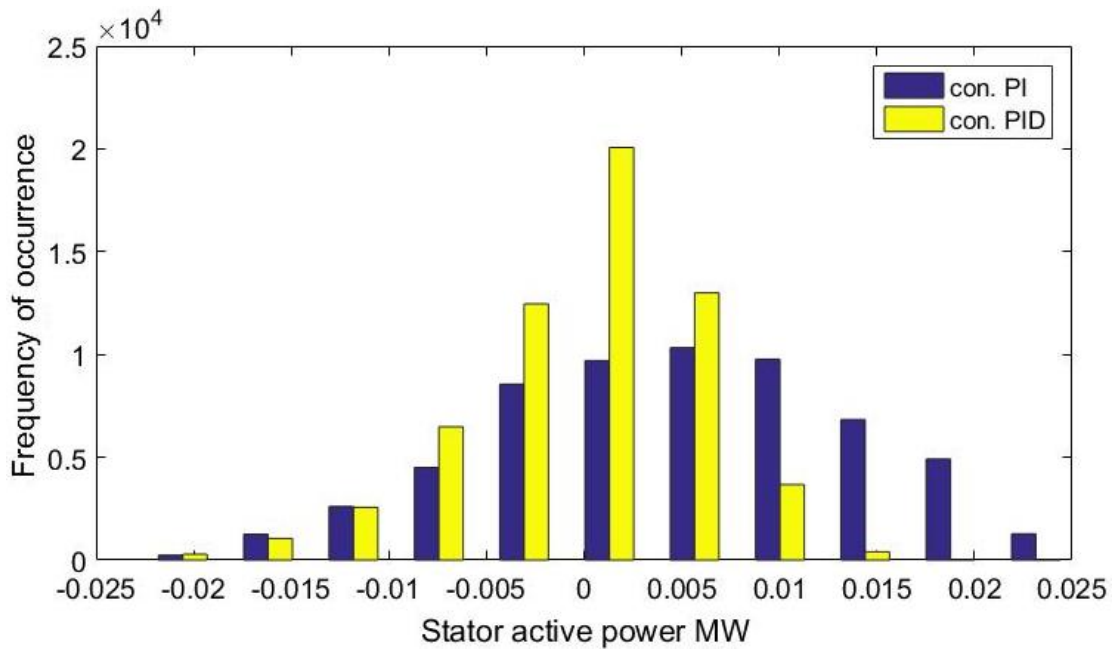Figure 4.10 Stator active power points above nominal value with different values of Kp and Ki

Figure 4.11 Histogram of ramp rate for stator power (MW) with different values of Kp and Ki

Table 4.3 Comparison of CVDPC- conventional PI-based and PID-based

CVDPC	Stator side		Rotor side	
	MW	%	MW	%
PI-based	0.028	0.37%	0.015	1.01%
PID-based with fixed PI coefficients	0.0135	0.16%	0.008	0.57%
PID-based with different values of PI coefficients	0.016	0.22%	0.011	0.78%

As seen from figures 4.9 and 4.10, the maximum value of stator active power for the CVDPC- conventional PID controller-based is (0.016MW) which represents (0.22%) of the nominal value, see table 4.3.

Hence, the CVDPC- conventional PID controller-based with different values of Kp and Ki gives smaller fluctuation compared with that of CVDPC- conventional PI controller-based by (41.54%), but it gives bigger fluctuation compared with that of CVDPC- conventional PID controller-based with identical Kp and Ki values by (18.52%).
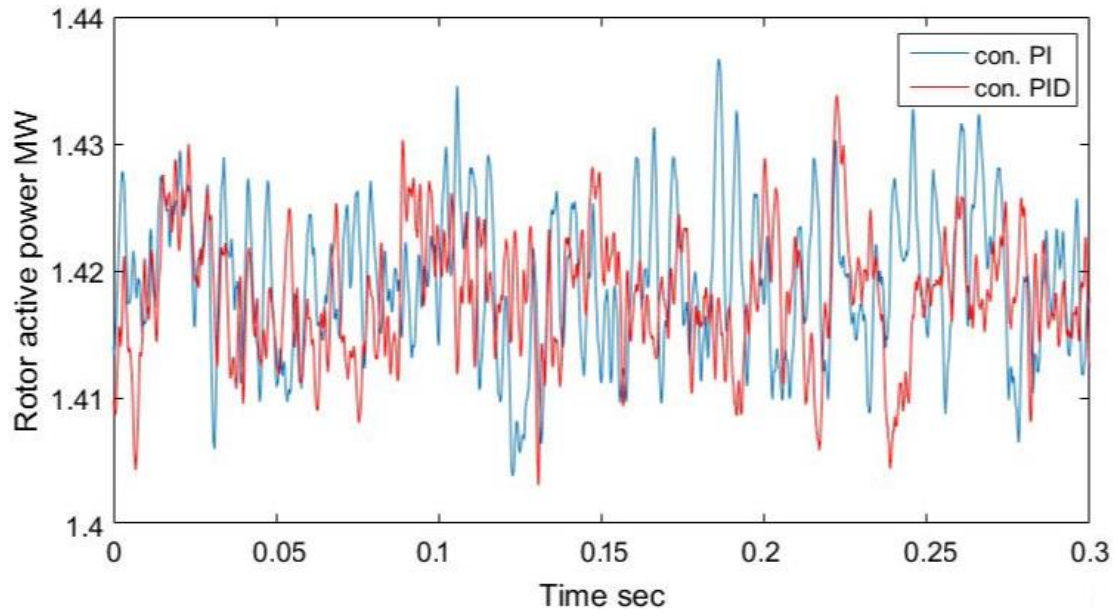
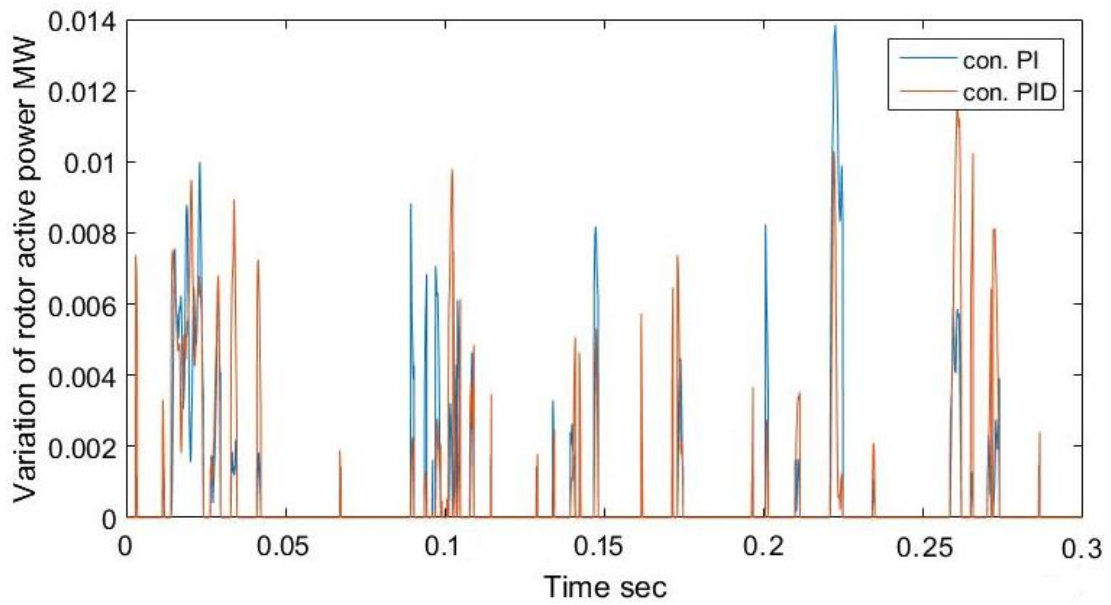Figure 4.12 Rotor active power with different values of Kp and Ki

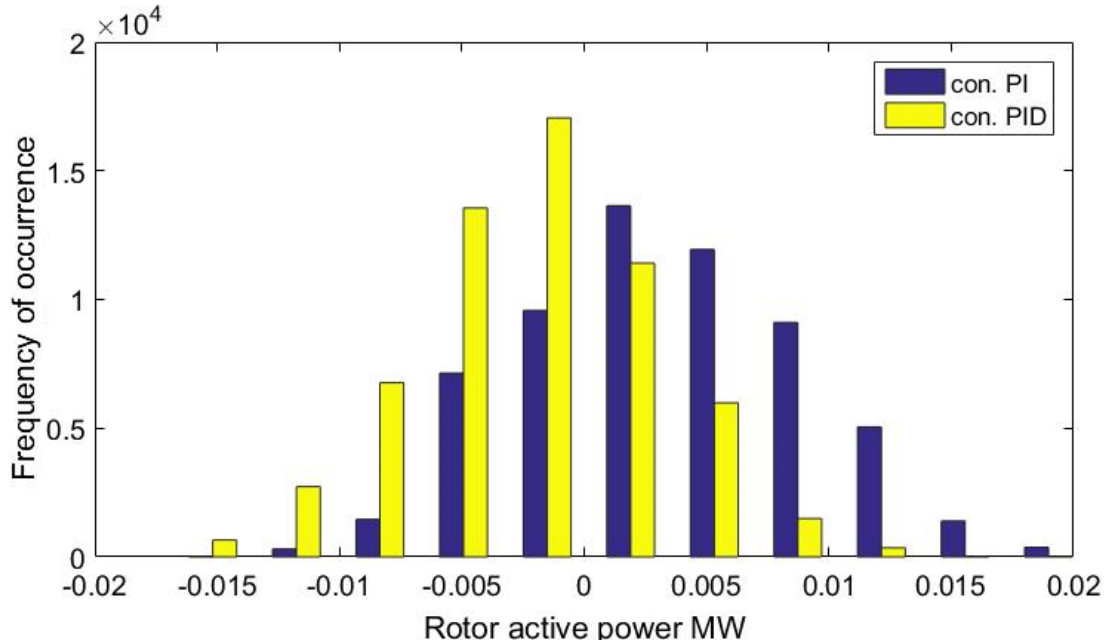Figure 4.13 Rotor active power points above nominal value

Figure 4.14 Histogram of ramp rate for rotor power (MW)

In the same manner, figures 4.12 and 4.13 show that the rotor active power reached (0.011MW) above the nominal value for CVDPC- conventional PID controller-based, which is (0.78%), see table 4.3 as well. So, the CVDPC- conventional PID controller-based with different values of Kp and Ki gives a smaller fluctuation compared to that of CVDPC-conventional PI controller-based by (22.77%), but it gives bigger fluctuation compared with that of CVDPC- conventional PID controller-based with identical Kp and Ki values by (37.5%).

Figures 4.11 and 4.14 show the location of each active power points for the CVDPC-conventional PI controller-based and CVDPC- conventional PID controller-based with, different values of Kp and Ki, and their distance from the nominal value, respectively.

As a conclusion, the system with conventional PID-based controller with identical values of Kp and Ki has more active power points located around the nominal value than that of

the system with conventional PI-based controller and with conventional PID-based controller with different values of Kp and Ki, hence, the use of conventional PID-based controller with identical values of Kp and Ki is the best in the steady-state condition.

4.2.3 Steady-State Condition of CVDPC Conventional PID-based and Adaptive PID-based

Following the same procedure that has been applied in the previous section, the maximum value that the stator has reached above the nominal value for the CVDPC- adaptive PID controller-based is (0.006MW) which represents (0.08%) of the nominal value of the stator active power, see figures 4.15 and 4.16. Whereas, as seen in the previous section, the maximum value of stator active power for the CVDPC- conventional PID controller-based is (0.016MW) which represents (0.22%) of the nominal value, see table 4.4.

Table 4.4 Comparison of CVDPC- conventional PI-based, PID-based and adaptive PID-based

CVDPC	Stator side		Rotor side	
	MW	%	MW	%
Conventional PI-based	0.028	0.37%	0.015	1.01%
Conventional PID-based with identical Kp and Ki	0.0135	0.16%	0.008	0.57%
Conventional PID-based with different Kp and Ki	0.016	0.22%	0.011	0.78%
adaptive PID-based	0.006	0.08%	0.007	0.49%

Hence, the CVDPC- adaptive PID controller-based gives a smaller fluctuation compared with that of CVDPC- conventional PID controller-based by about (62.5%) and by (78.6%) for CVDPC- conventional PI controller-based.
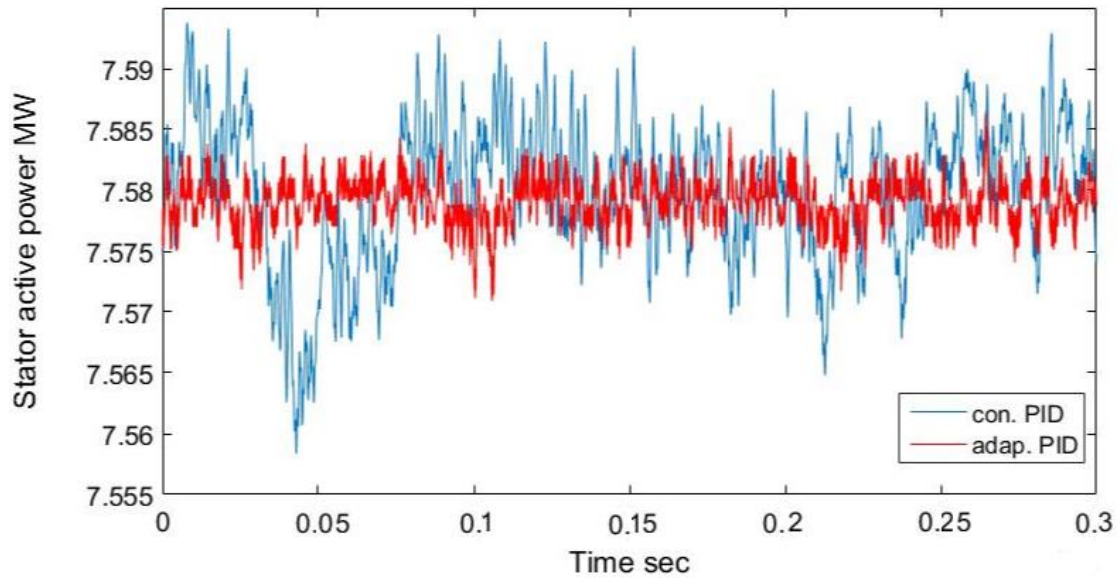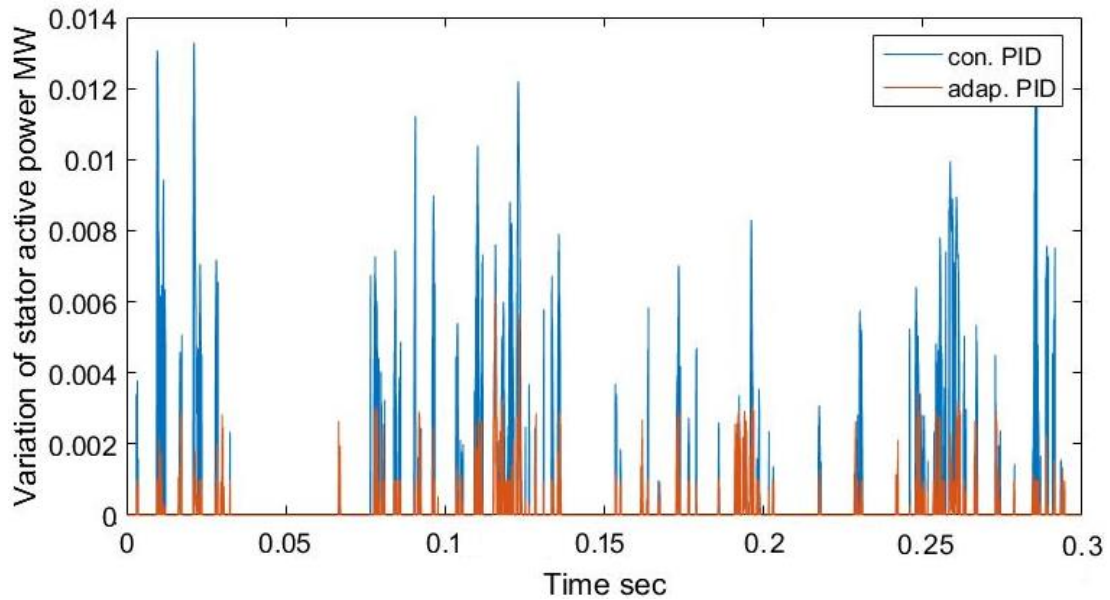

Figure 4.15 Stator active power

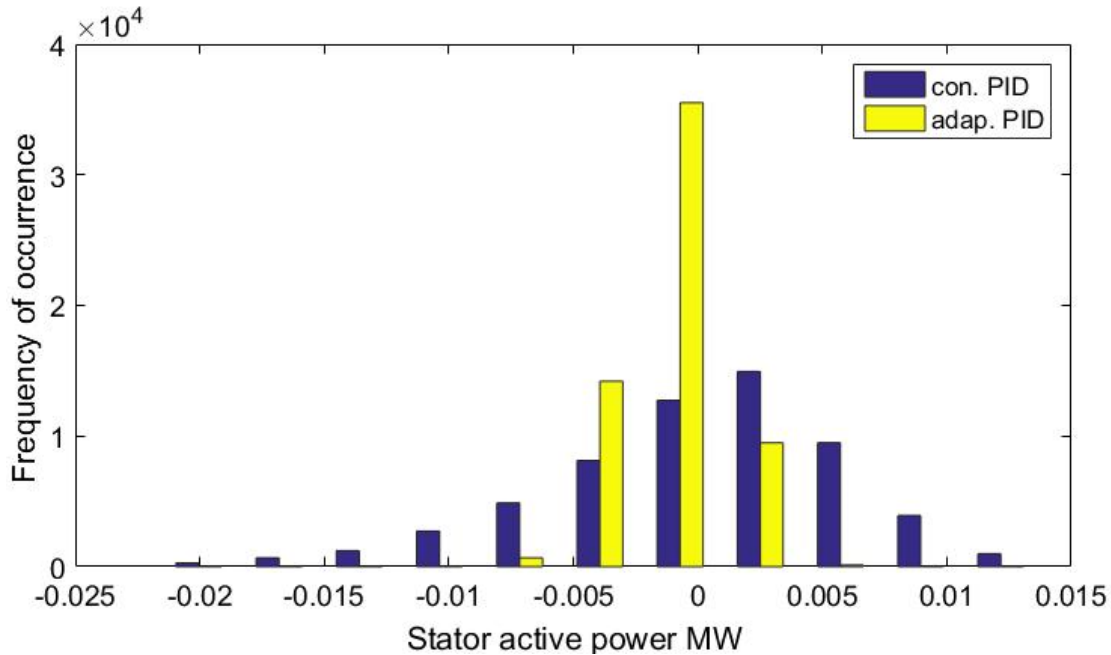Figure 4.16 Stator active power points above nominal value

Figure 4.17 Histogram of ramp rate for stator power (MW)

Also, figures 4.18 and 4.19 show that the rotor active power reached (0.007MW) above the nominal value for CVDPC- adaptive PID controller-based which represents (0.49%), see table 4.4 as well. So, the CVDPC- adaptive PID controller-based gives a smaller fluctuation compared with that of CVDPC- conventional PID controller-based by about (37.2%) and by (53%) for CVDPC- conventional PI controller-based.

Similarly, figures 4.17 and 4.20 illustrate the location of each active power points for the proposed CVDPC- adaptive PID-based controller and CVDPC- conventional PID-based controller and their distance from the nominal value, respectively. The greater the number of active power points are close to the nominal value the more the system is optimal. As seen, the system with the proposed controller has more active power points around the nominal value, hence, the proposed controller is better than conventional PI-based and conventional PID-based.
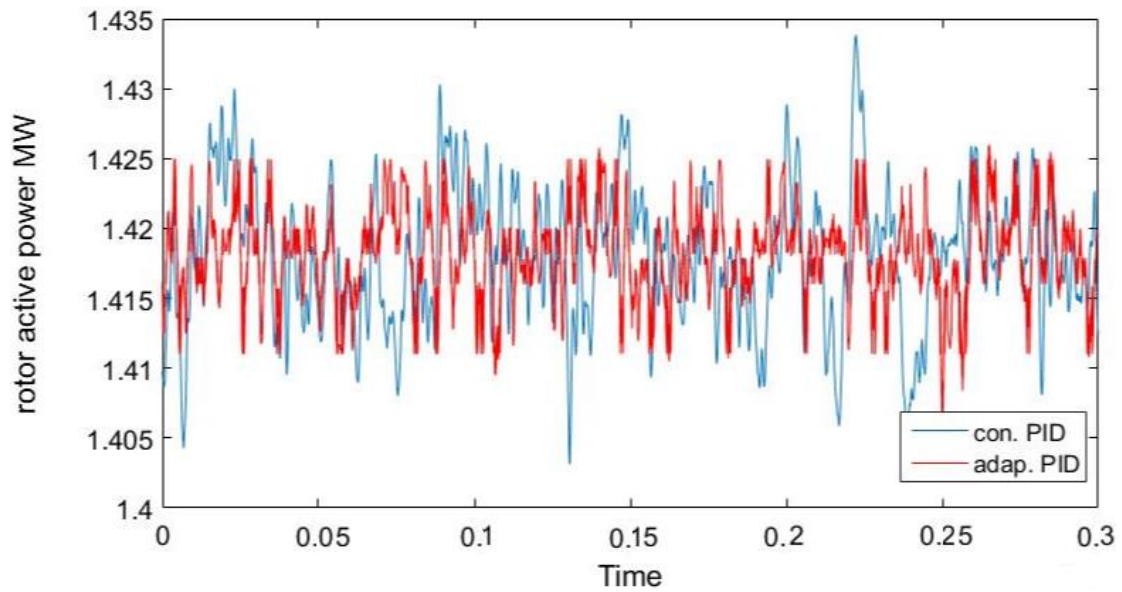
Figure 4.18 Rotor active power
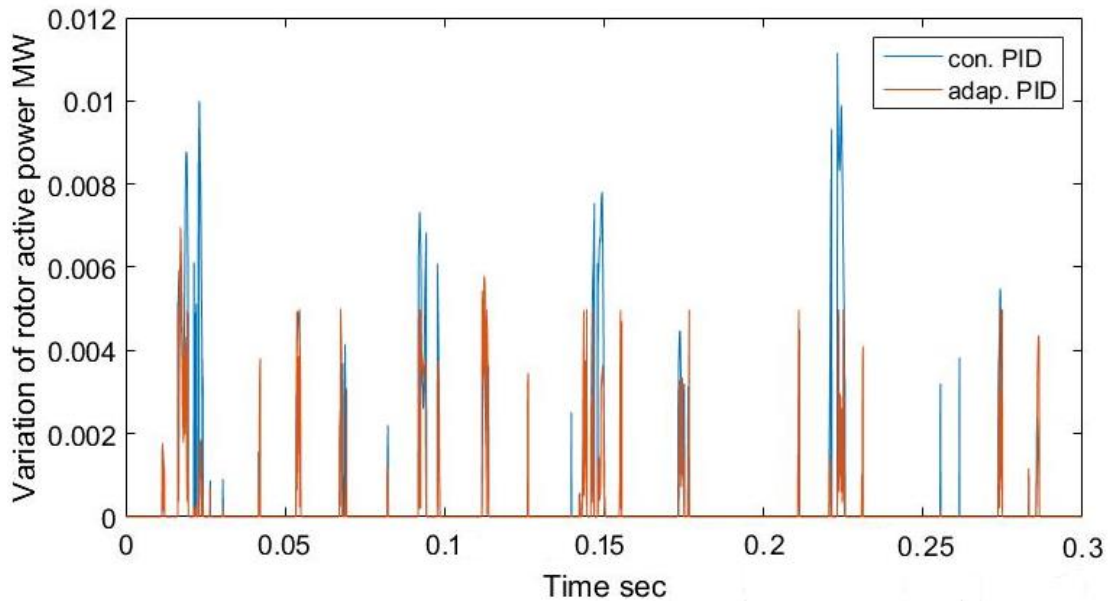
Figure 4.19 Rotor active power points above nominal value
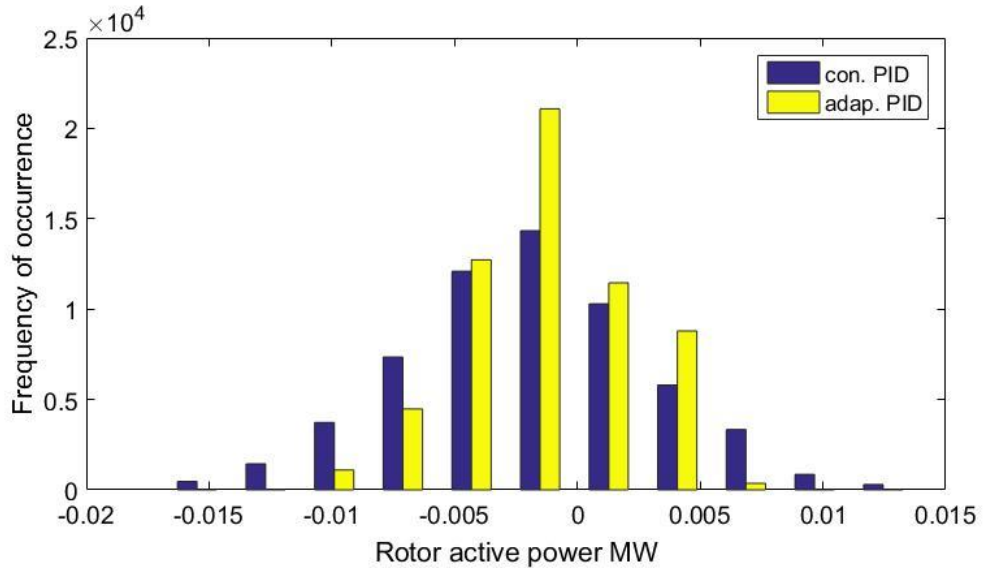
Figure 4.20 Histogram of ramp rate for rotor power (MW)

Figure 4.21 and 4.22 illustrate the adaptive PID coefficients' values during the steady-state condition and generated by model reference adaptive control MRAC and applied on the CVDPC system. The figures include the values of Kp, Ki and Kd.
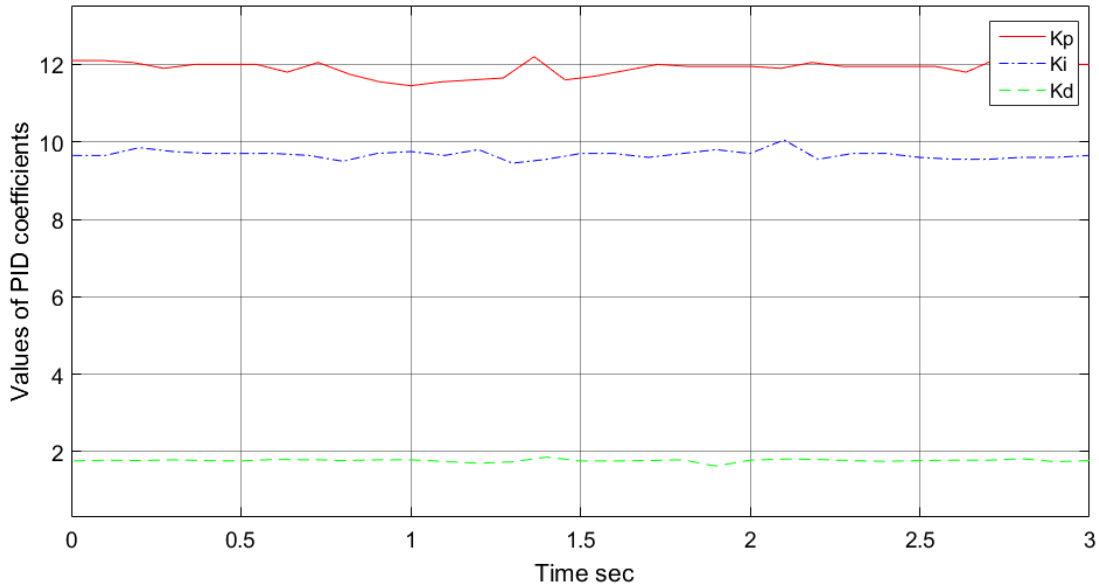
Figure 4.21 The values of adaptive PID coiffecients for (Idr) during steady-state condition
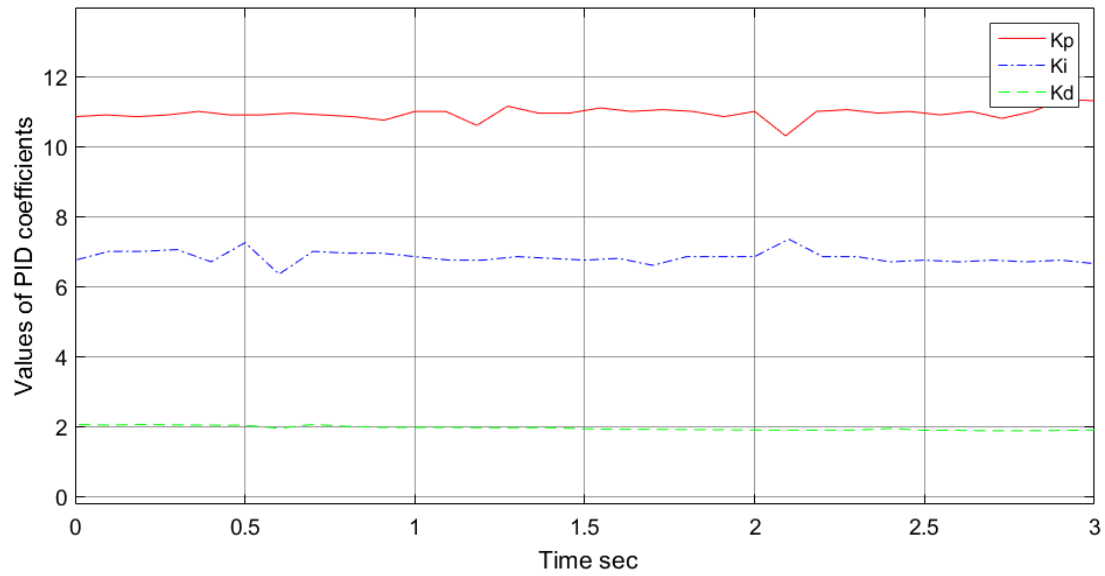
Figure 4.22 The values of adaptive PID coeffocoents for (Iqr) during steady-state condition

Figure 4.23 Stator reactive power of CVDPC conventional PID-based and adaptive PID-based

Figure 4.23 illustrates the stator reactive power of the CVDPC controller conventional PID-based and adaptive PID-based and, as seen, the stator reactive power is equal to zero, as expected. That is due to the ultimate use of the current capability of RSC for generating active power, the stator reactive power output of the system is zero [24].

4.3   Transient Condition

4.3.1   Rotor Resistance Changing R_r

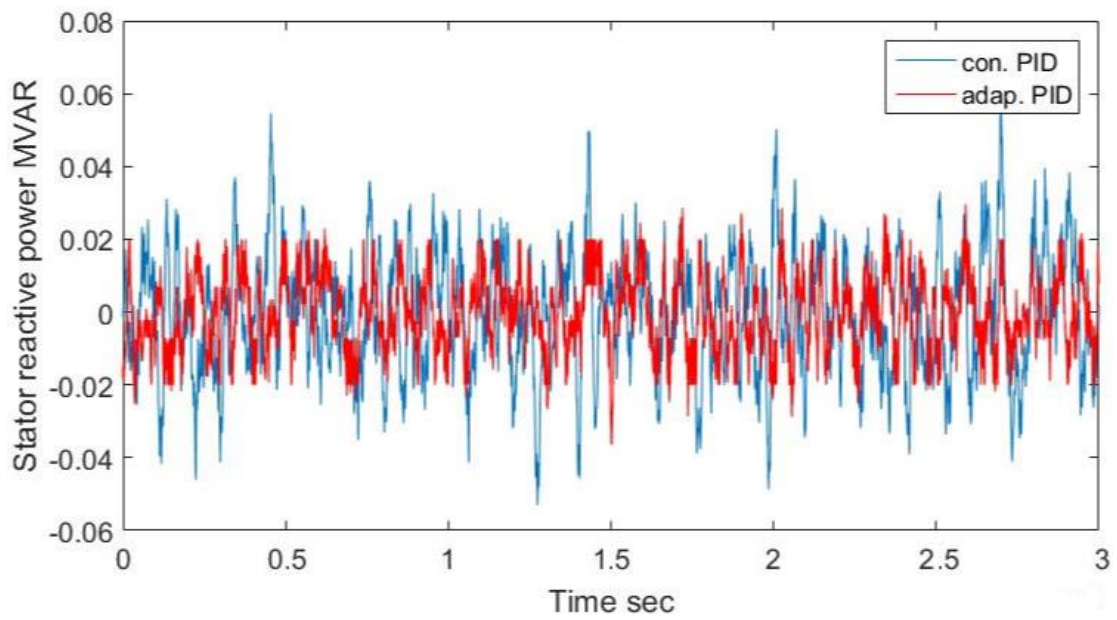Changing the rotor resistance Rr is suggested in order to investigate the system behavior under dynamic response and extreme events. The following figures 4.24 - 4.26 show the simulation results according to this condition.

At t=0.25 s, the value of rotor resistance Rr is changed to be higher by four times over the current value. In addition, this part illustrates the robustness of the system during the parameters variation.

4.3.1.1   Transient Condition of CVDPC Conventional PI-based and Conventional PID-based with identical PI coefficients

Figures 4.24 - 4.29 illustrate the effect of increasing rotor resistance Rr. The total, stator and rotor active power of the system has been experienced the transient state before returning back to the steady-state condition. The total active power decreases from 9 to 8.67 MW and the stator active power rises from 7.58 to 7.86 MW. In other hand, the rotor active power reduces from 1.42 to 1.14 MW, while the stator reactive power does not

change during all cases due to the ultimate use of the current capability of RSC for generating active power.

Figure 4.24 Total active power for CVDPC- conventional PI and conventional PID based with iddntical values of Kp and Ki

Figure 4.24 shows the case of changing the value of rotor resistance for the total active power of the system for CVDPC- conventional PI controller-based and conventional PID controller-based with similar values of Kp and Ki. As a result, the settling time of the case of CVDPC- conventional PI-based controller is $t_s = 1.85\ s$, whereas that for CVDPC-conventional PID-based controller is about $t_s = 2\ s$, see table 4.5. So, when the values of Kp and Ki are chosen to be similar for both controllers, the system starts to return to its nominal value and the response of the proposed controller is slower than the CVDPC-conventional PI-based controller by about 8.1%.

Table 4.5 The settling time of CVDPC- conventional PI-based and PID-based

CVDPC	PI-based	PID-based with identical values of Kp and Ki
settling time t_s (seconds)	1.85	2

Figure 4.25 Stator active power for CVDPC- conventional PI and conventional PID based with identical values of Kp and Ki

The same behavior is found for the stator active power of the system for both CVDPC-conventional PI controller-based and conventional PID controller-based, see figure 4.25.

And for the rotor active power, the behavior of both controllers is approximately the same as expected, see figures 4.26 and 4.29.
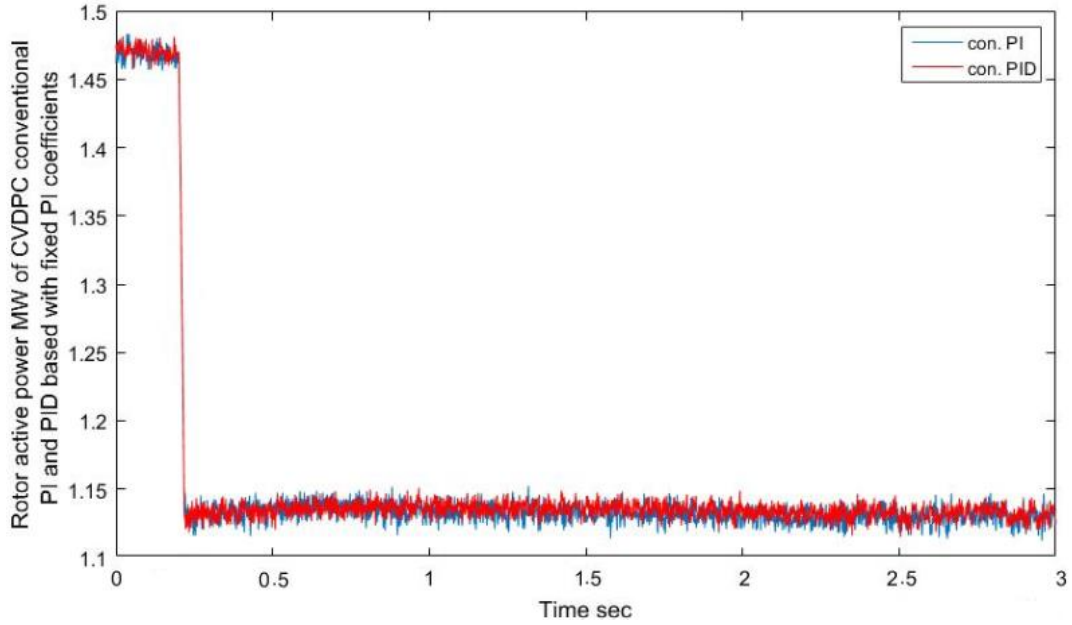
Figure 4.26 Rotor active power for CVDPC- conventional PI and PID based with fixed values of Kp and Ki

4.3.1.2 Transient Condition of CVDPC Conventional PI-based and Conventional PID-based with different PI coefficients
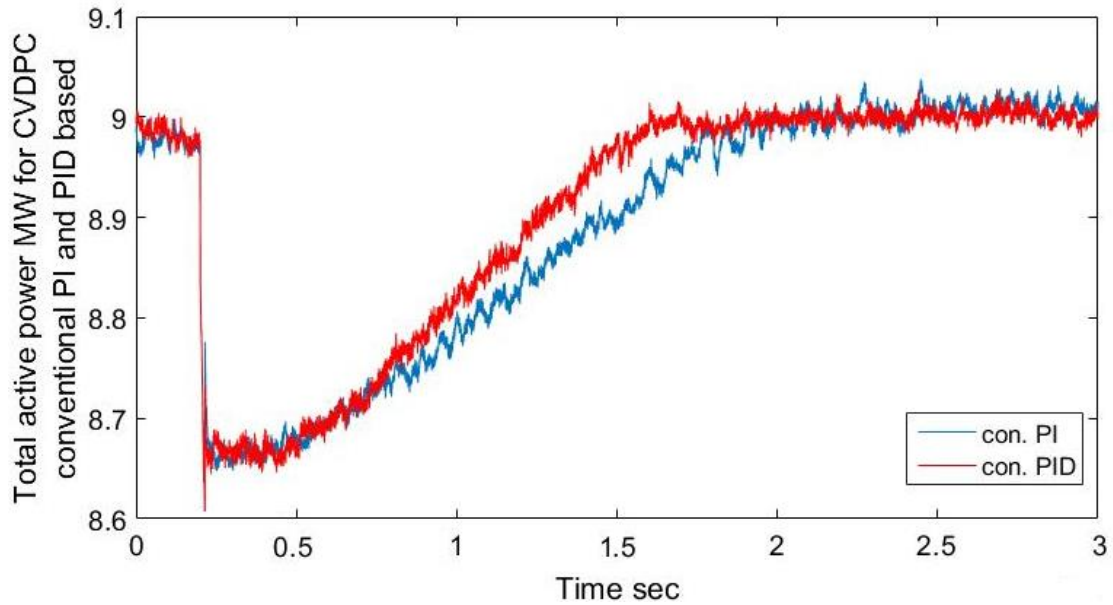
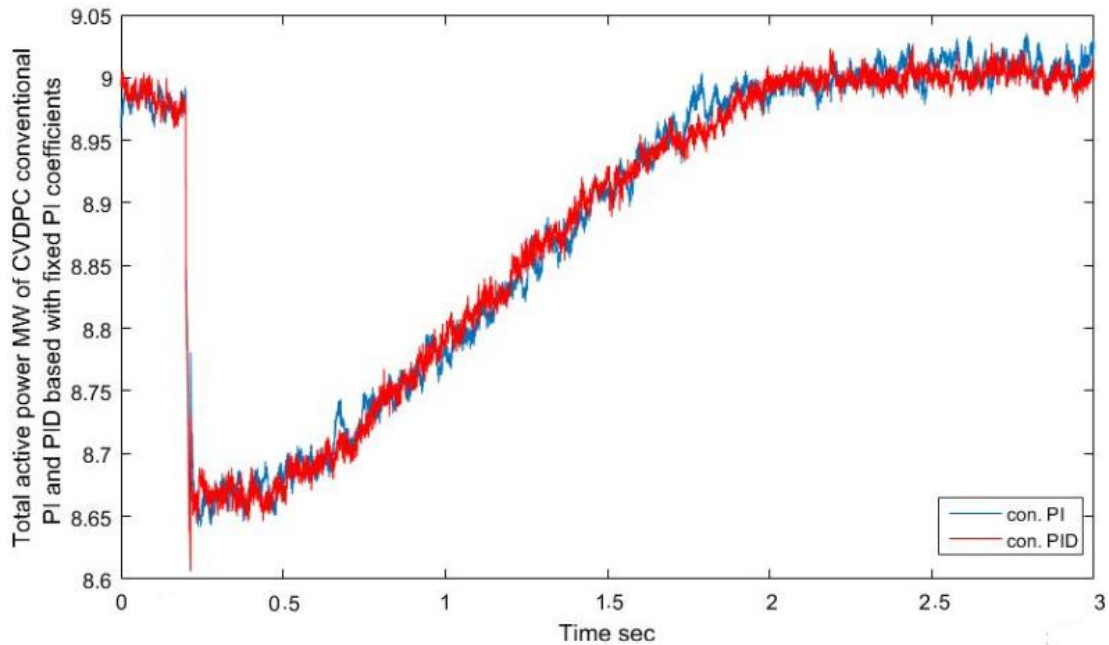Figure 4.27 Total active power for CVDPC- conventional PI and conventional PID based with different values of Kp and Ki

Figure 4.27 shows the case of changing the value of rotor resistance for the total active power of the system for CVDPC- conventional PI controller-based and conventional PID controller-based with different values of Kp and Ki. In this case, the settling time of the case of CVDPC- conventional PID-based controller is $t_s = 1.5\ s$, see table 4.6. So, the system starts to return to its nominal value and the response of the proposed controller is faster than the CVDPC- conventional PI-based controller by about 19% and then the CVDPC- conventional PID-based controller with similar values of Kp and Ki by about 19%.

Table 4.6 The settling time of CVDPC- conventional PI-based and PID-based

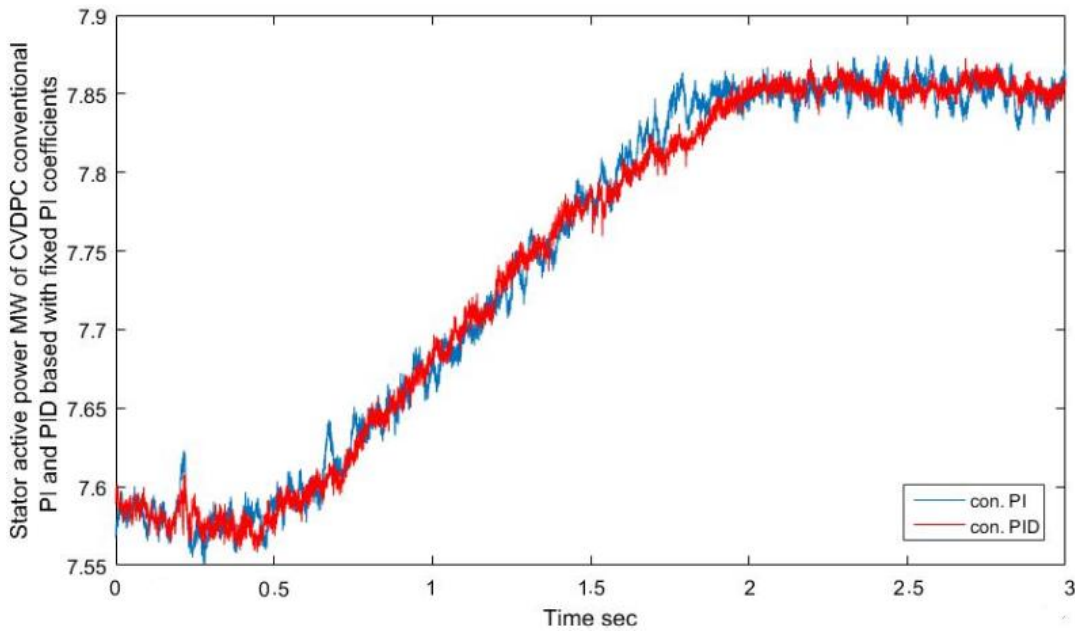| CVDPC	PI-based	PID-based with identical Kp and Ki	PID-based with different Kp and Ki
settling time t_s (seconds)	1.85	2	1.5

Figure 4.28 Stator active power for CVDPC- conventional PI and conventional PID based with different values of Kp and Ki

The same behavior is found for the stator active power of the system for both CVDPC-conventional PI controller-based and conventional PID controller-based, see figure 4.28.
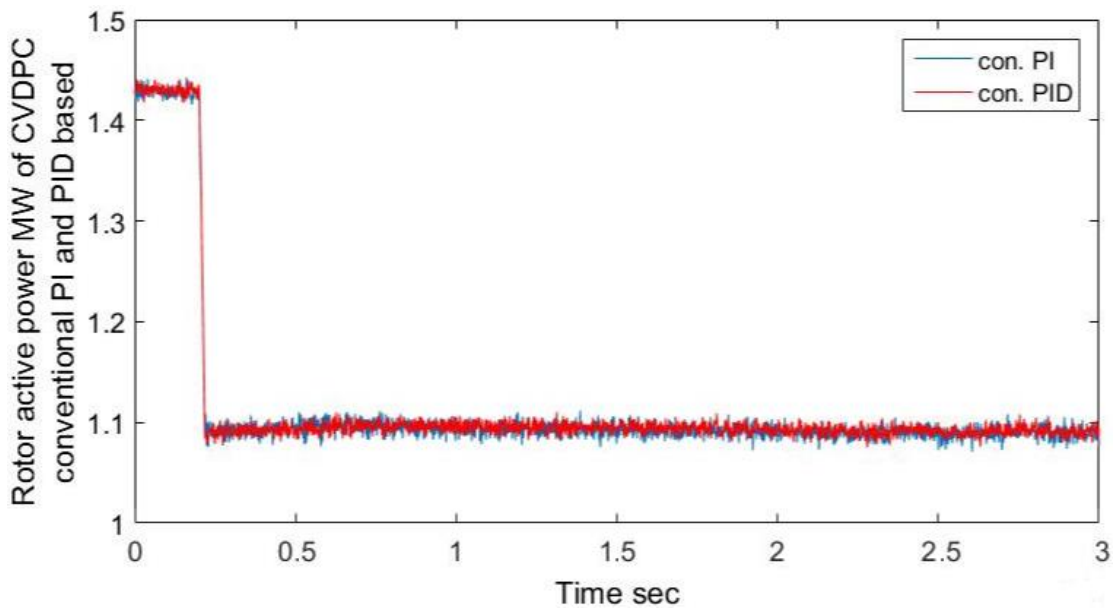
Figure 4.29 Rotor active power for CVDPC- conventional PI and PID based with different values of Kp and Ki

And for the rotor active power, the behavior of both controllers is approximately the same as expected, see figures 4.26 and 4.29.
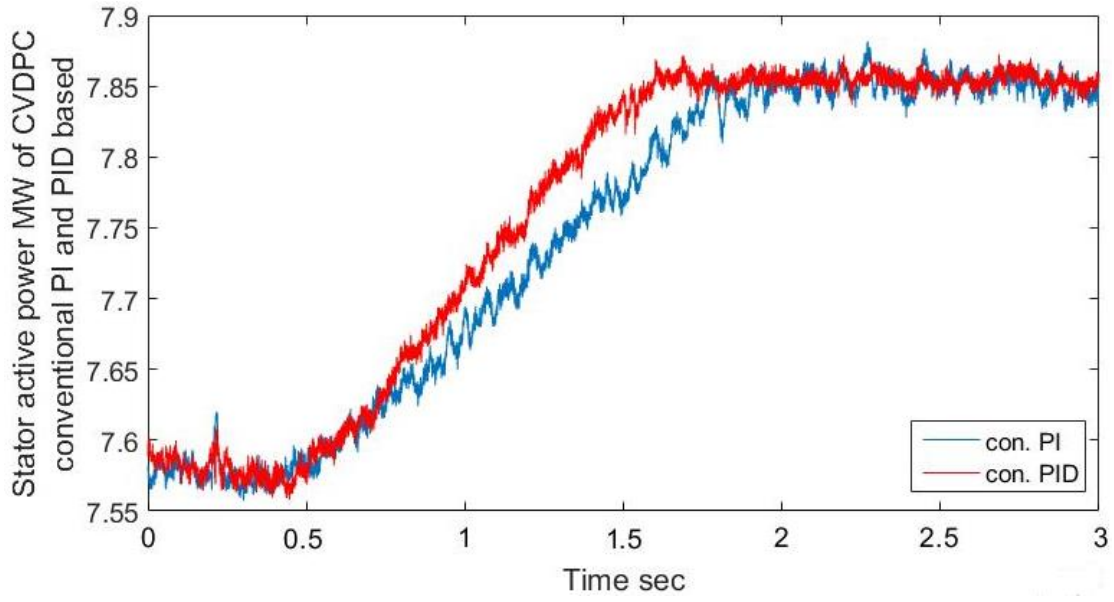
By comparing table 4.3 and 4.6, it is easy to conclude that, the system with conventional PID-based controller with different values of Kp and Ki is more robust during parameter variation and gives reasonable behavior during steady-state condition.

4.3.1.3   Transient Condition of CVDPC Conventional PID-based and Adaptive PID-based

In this part, figures 4.30 and 4.31 present the case of changing the value of rotor resistance for the total active power of the system for CVDPC- conventional PID-based controller and adaptive PID-based controller. As a result, the settling time of the case of CVDPC- conventional PID-based controller is $t_s = 1.5\ s$ as seen previously, whereas that for CVDPC- adaptive PID-based controller is about $t_s = 1.1\ s$, see table 4.7.

Table 4.7 The settling time of CVDPC- conventional PI-based, PID-based and adaptive PID-based

CVDPC	Conventional PI-based	Conventional PID-based	Adaptive PID-based
settling time t_s (seconds)	1.85	1.5	1.1

So, the system starts to return to its nominal value and the response of the proposed controller is faster than the CVDPC- conventional PID-based controller by about 26.7% and then that of the CVDPC- conventional PI-based controller by about 40.5%.
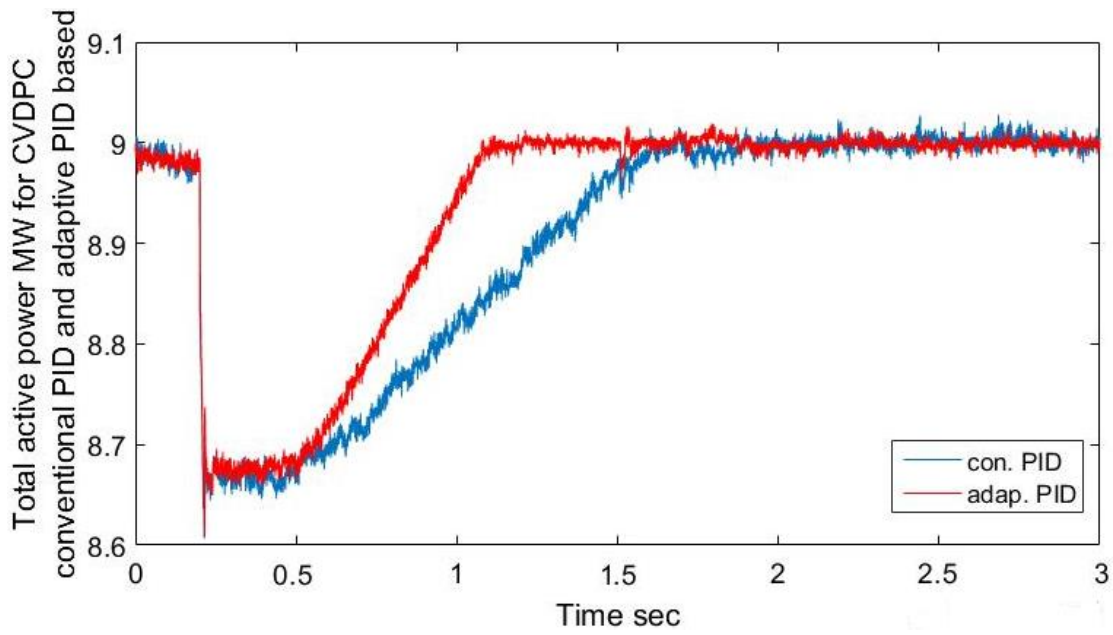
Figure 4.30 Total active power for CVDPC- conventional PID-based and adaptive PID-based
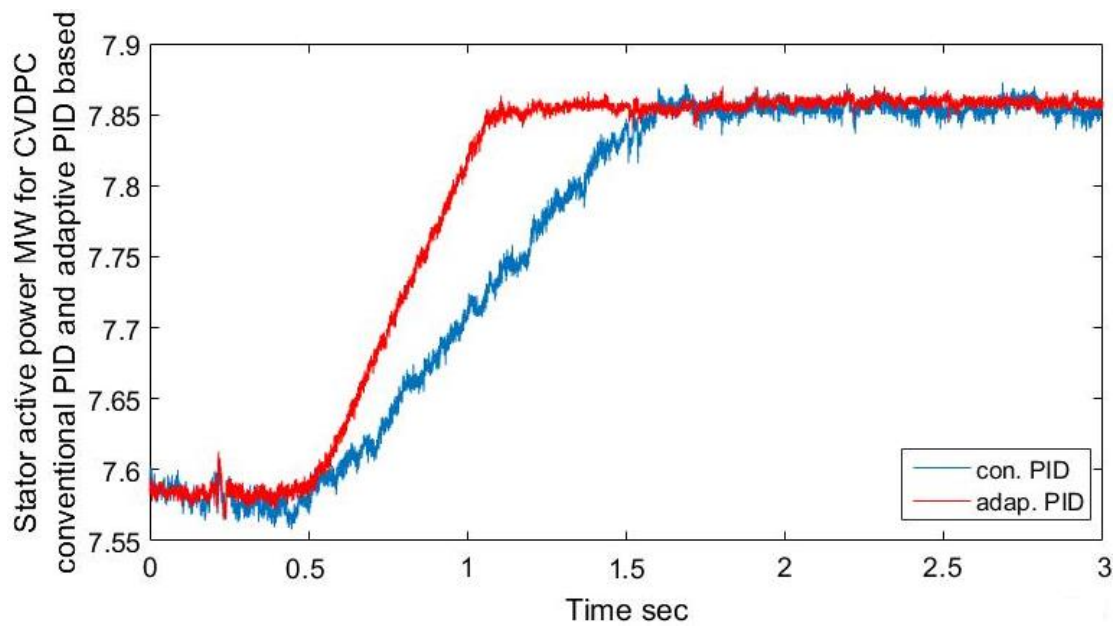
Figure 4.31 Stator active power for CVDPC- conventional PID-based and adaptive PID-based

And for the rotor active power, the behavior of all controller cases is the same as expected, see figures 4.26, 4.29 and 4.32.
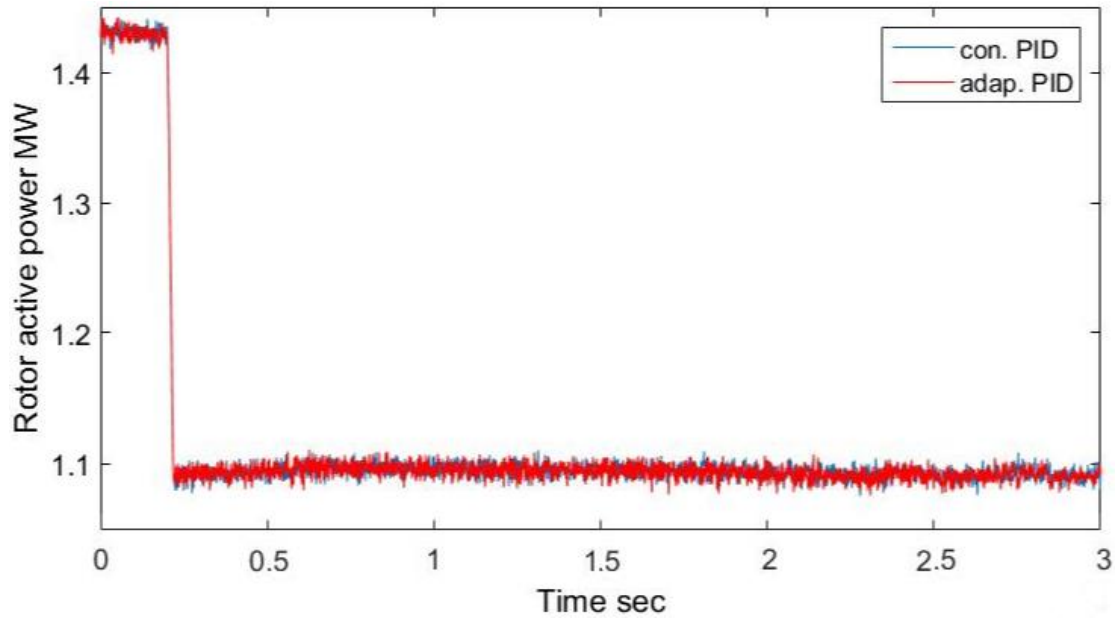
Figure 4.32 Rotor active power for CVDPC- conventional PID-based and adaptive PID-based

Figures 4.33 and 4.34 illustrate the adaptive PID parameters' values during the transient condition and obtained by model reference adaptive control MRAC and applied on the CVDPC system. The figures include the values of Kp, Ki and Kd.
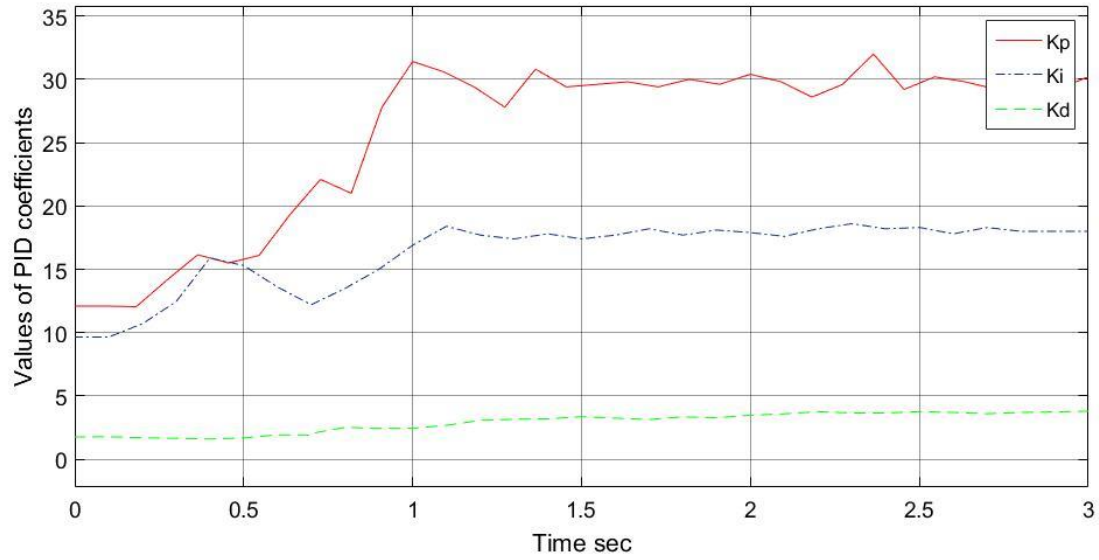
Figure 4.33 The values of adaptive PID coefficients for (idr) during transient condition
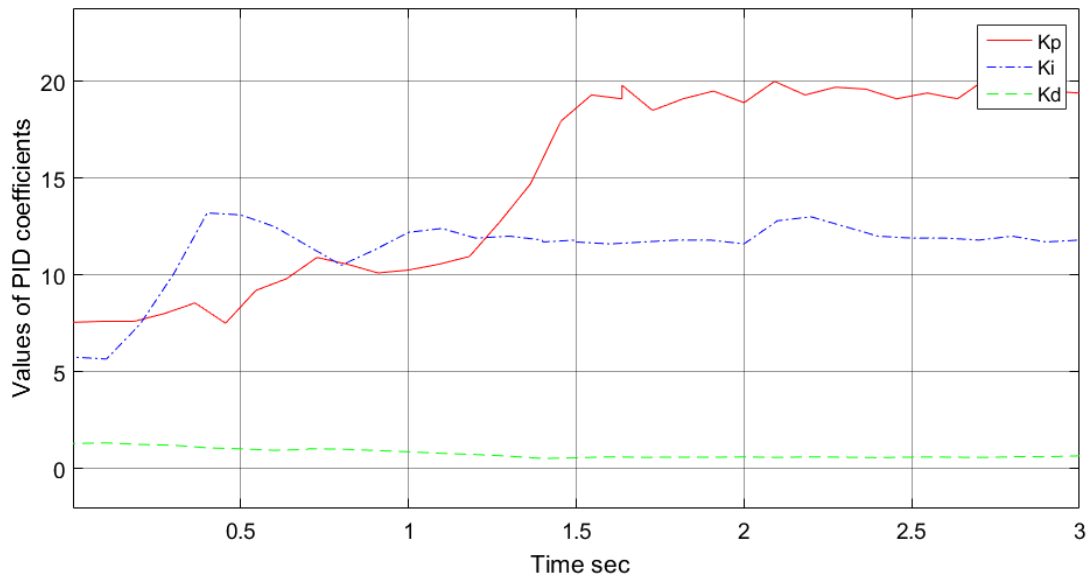
Figure 4.34 The values of adaptive PID coefficients for (iqr) during transient condition

4.3.2   Wind Speed Disturbance

In this section of the evaluation, the wind speed is changed in order to check the system transient conditions and the compression has been achieved for the CVDPC conventional PI-based, PID-based and adaptive PID-based controllers. Figures 4.35 – 4.38 illustrate the simulation results of this evaluation part. At t = 0.32s, the wind speed step decreases suddenly from 15m/s to 10m/s and, see figure 4.35.
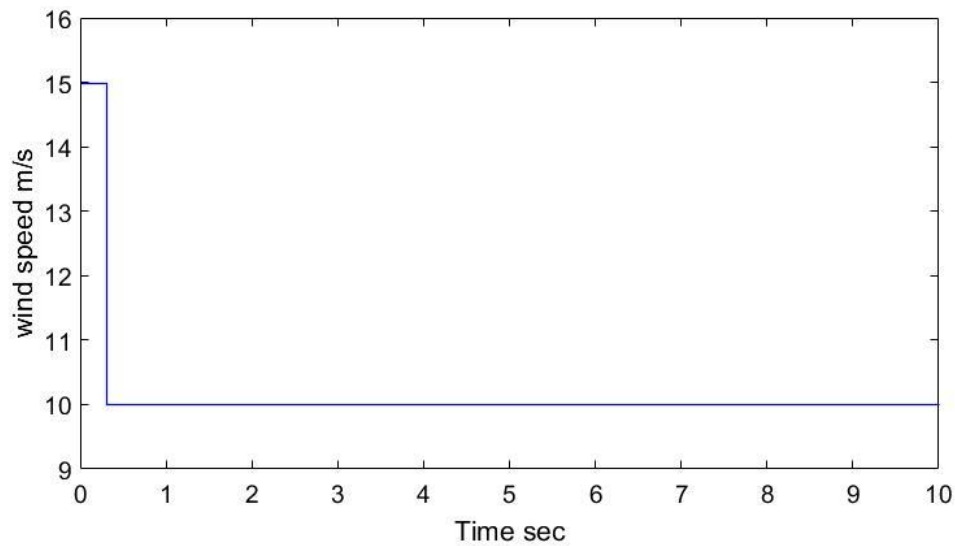
Figure 4.35 Wind speed disturbance

As a result, the rotor speed goes down to 0.8p.u. from 1.2p.u., see figure 4.36. In the same vein, figure 4.37 shows that the production of the stator active power reduces from 7.85 MW to 2.8 MW and 20% of the stator active power is fed back to the machine via the converters (p_r= -0.6 MW).
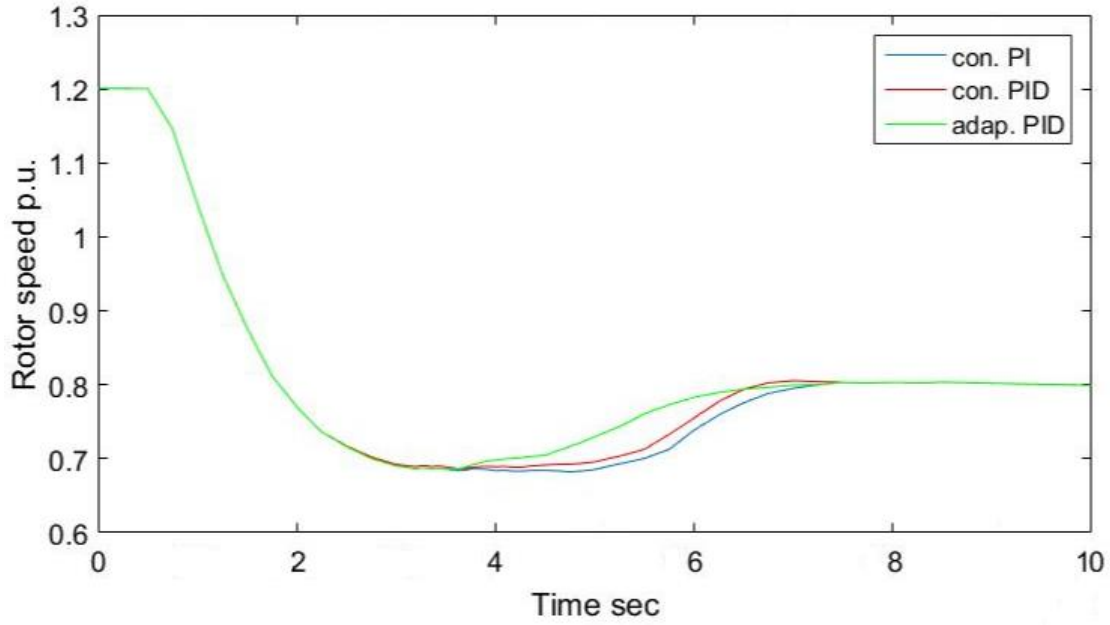
Figure 4.36 Rotor speed (w_r) during wind speed variation
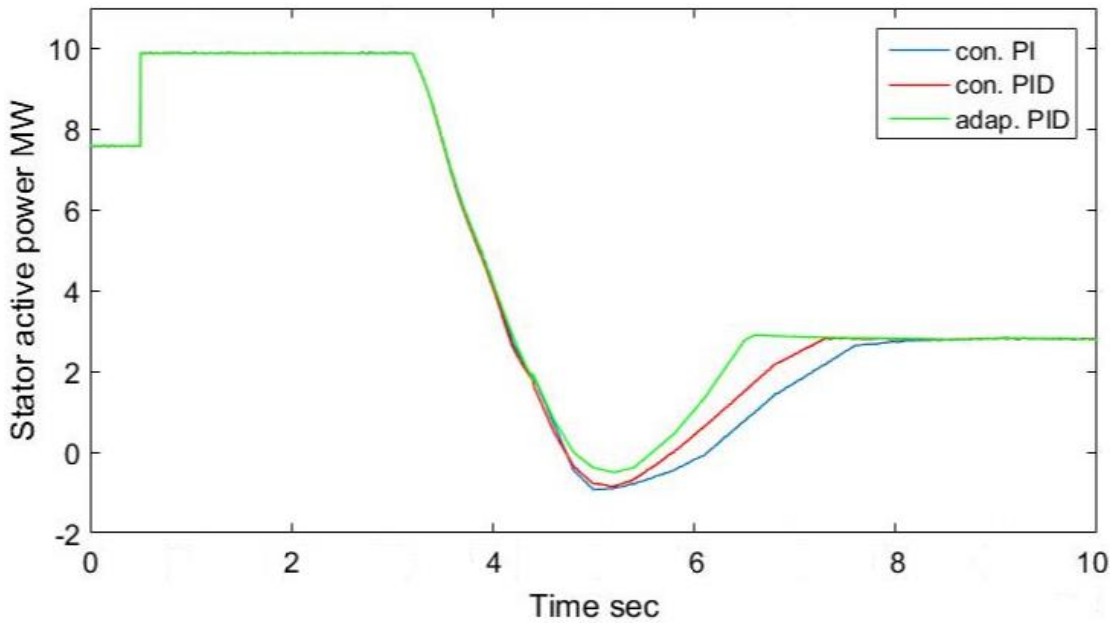
Figure 4.37 Stator active power during wind speed disturbance
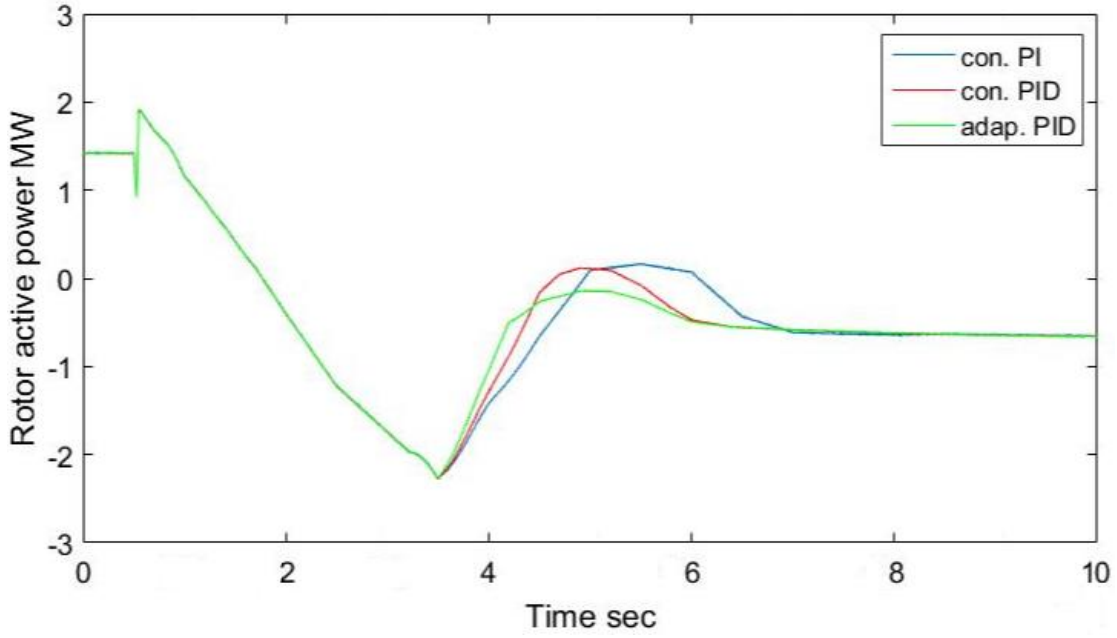
Figure 4.38 Rotor active power during wind speed variation
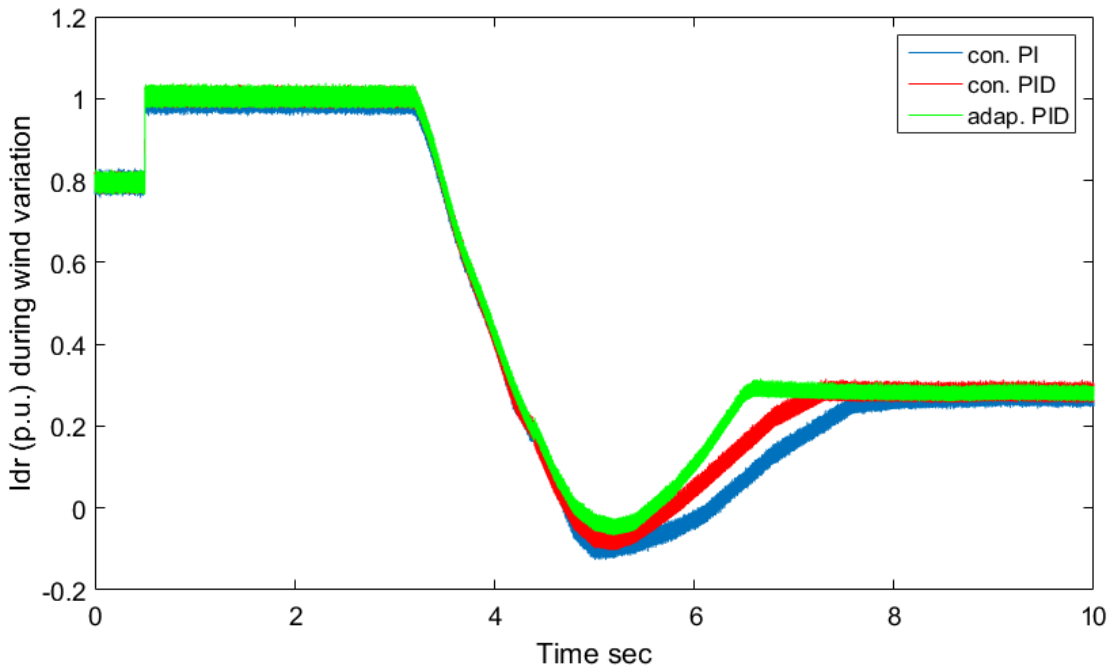
Figure 4.39 Rotor current Idr (p.u.) during wind speed changing

Figures 4.36 – 4.39 show that, the generator is in steady state condition where the wind speed is 15m/s and rotor speed is 1.2p.u., but suddenly, wind speed drops to 10m/s and rotor speed starts to decrease gradually. The controller detects the sudden drop in wind speed and starts to increase the stator active power to about 9.8MW by increasing rotor current Idr. Since rotor speed is decreasing very slowly due to the inertia of the turbine, the rotor active power will decrease accordingly, and the stator active power is almost remaining the same until the rotor active power reaches zero, then the rotor starts to absorb power from the grid till about 2MW.

At this point, the stator active power decreases, and the rotor active power starts to increase. Following the same behavior, the stator active power reduces until it reaches zero, then it starts to absorb power from the grid which means that the generator acts as a motor. Consequently, the rotor speed keeps increasing.

The system returns to its steady-state condition and the values of generator becomes as following: the stator provides (generate) 2.8MW and the rotor absorb (consume) 0.6MW.

As seen, it can be concluded that the response of CVDPC during wind speed disturbance is better when the adaptive PID controller is handled. So, the system is more robust and faster in response when the proposed CVDPC adaptive PID- based is used in the wind energy farm.

CHAPTER 5

CONCLUSION and RECOMMENDATION

5.1   CONCLUSION

In conclusion, the combined vector and direct power control CVDPC is a control system that attains the advantages of two controllers: vector control CV and direct power control DPC. These advantages include lower power ripple, lower harmonic distortion, robust against parameter variations and rapid dynamic responses. The use of conventional (PI) controller in CVDPC is necessary in order to guarantee the stability of system even though it will affect the quality of performance of the system. In this thesis, the model reference adaptive controller MRAC is used to optimize the coefficients of the PID controller adaptively. The performance of the proposed controller (CVDPC adaptive PID-based) is compared with that of the CVDPC based on conventional PI and PID controllers by studying the steady-state and transient conditions of the output power of the system. Simulation results showed clearly that the proposed controller has a superior performance compared to the other controllers in damping power oscillation and improving the transient stability and the robustness of the DFIG systems when they are subjected to external disturbances. The CVDPC adaptive PID-based controller demonstrated a satisfying system performance by lowering the power ripple, achieving high dynamic response and increasing the system robustness under both steady-state and transient conditions, even with parameter variations.

5.2   FUTURE WORK

This work can be extended and examined using several ways such as,

1- applying real wind speed data instead of using fixed values of wind speed to examine the system response and robustness.

2- The simulation can be done with other scenarios of adaptive controllers such as particle swarm optimization PSO in order to speed up and minimize the simulation time.

References

[1] M. Mohseni, S. Islam, and M. A. S. Masoum, "Enhanced hysteresis- based current regulators in vector control of DFIG wind turbines," IEEE Trans. Power Electron., vol. 26, no. 1, pp. 223–234, Jan. 2011.

[2] G. Abad, J. Lopez, M. A. Rodriguez, L. Marroyo, and G. Iwanski, Doubly Fed Induction Machine Modeling and Control for Wind Energy Generation Applications. Hoboken, NJ, USA: Wiley, 2011.

[3] H. M. Jabr, D. Lu, and N. C. Kar, "Design and implementation of neurofuzzy vector control for wind driven doubly fed induction generator," IEEE Trans. Sustain. Energy, vol. 2, no. 4, pp. 404–413, Oct. 2011.

[4] S. Li, T. A. Haskew, K. A. Williams, and R. P. Swatloski, "Control of DFIG wind turbine with direct-current vector control configuration," IEEE Trans. Sustain. Energy, vol. 3, no. 1, pp. 1–11, Jan. 2012.

[5] J. P. A. Vieira1, M. V. A. Nunes, U. H. Bezerra, and A. C. Nascimento, "Designing optimal controllers for doubly fed induction generators using a genetic algorithm," IET Gen. Transm. Distrib., vol. 3, no. 5, pp. 472–484, May 2009.

[6] L. Xu and P. Cartwright, "Direct active and reactive power control of DFIG for wind energy generation," IEEE Trans. Energy Convers., vol. 21, no. 3, pp. 750–758, Sep. 2006.

[7] J. Hu, H. Nian, B. Hu, and Y. He, "Direct active and reactive power regulation of DFIG using sliding-mode control approach," IEEE Trans. Energy Convers., vol. 25, no. 4, pp. 1028–1039, Dec. 2010.

[8] G. Abad, M. A. Rodriguez, and P. Poza, "Two-level VSC-based predictive direct power control of the doubly fed induction machine with reduced power ripple at low constant switching frequency," IEEE Trans. Energy Convers., vol. 23, no. 2, pp. 570–580, Jun. 2008.

[9] A. J. Sguarezi Filho and E. R. Filho, "Model-based predictive control applied to the doubly-fed induction generator direct power control," IEEE Trans. Sustain. Energy, vol. 3, no. 3, pp. 398–406, Jul. 2012.

[10] J. Hu, J. Zhu, Y. Zhang, and G. Platt, "Predictive direct virtual torque and power control of doubly fed induction generators for fast and smooth grid synchronization and flexible power regulation," IEEE Trans. Power Electron., vol. 28, no. 7, pp. 3182–3194, Jul. 2013.

[11] S. Vaez-Zadeh and E. Daryabeigi, "Combined vector and direct torque control methods for IPM motor drives using emotional controller (BELBIC)," in Proc. 2nd Power Electron., Drive Syst. Technol. Conf. (PEDSTC), Tehran, Iran, 2011, pp. 145–150.

[12] S. Vaez-Zadeh and R. Shafaie, "Toward a common framework for analysis of high performance controls of PMS motor drives," in Proc. 2nd Power Electron., Drive Syst. Technol. Conf. (PEDSTC), Tehran, Iran, Feb. 2011, pp. 241–245.

[13] S. Vaez-Zadeh and E. Jalali, "Combined vector control and direct torque control method for high performance induction motor drives," Energy Convers. Manage., Elsevier, vol. 48, no. 12, pp. 3095–3101, Dec. 2007.

[14] Z. Boulghasoul, A. Elbacha, E. Elwarraki, and D. Yousfi, "Combined vector control and direct torque control an experimental review and evaluation," in Proc. Int. Conf. Multimedia Comput. Syst. (ICMCS), Ouarzazate, Morocco, 2011, pp. 1–6.

[15] M. Farasat and E. Karaman, "Efficiency-optimized hybrid field oriented and direct torque control of induction motor drive," in Proc. Int. Conf. Electr. Mach. Syst. (ICEMS), Beijing, China, Aug. 2011, pp. 1–4.

[16] Karimi, Hossein, Sadgeh Vaez-Zadeh, and Farzad Rajaei Salmasi. "Combined vector and direct thrust control of linear induction motors with end effect compensation." IEEE Transactions on Energy Conversion 31.1 (2016): 196-205.

[17] Sayritupac, José, et al. "Predictive control strategy for dfig wind turbines with maximum power point tracking using multilevel converters." Power Electronics and Power Quality Applications (PEPQA), 2015 IEEE Workshop on. IEEE, 2015.

[18] Li, Shuhui, et al. "Control of DFIG wind turbine with direct-current vector control configuration." IEEE transactions on Sustainable Energy 3.1 (2012): 1-11.

[19] Hu, Jiabing, and Xiaoming Yuan. "VSC-based direct torque and reactive power control of doubly fed induction generator." Renewable energy 40.1 (2012): 13-23.

[20] Errouissi, Rachid, et al. "Offset-free direct power control of dfig under continuous-time model predictive control." IEEE Transactions on Power Electronics 32.3 (2017): 2265-2277.

[21] Amrane, Fayssal, Azeddine Chaiba, and Saad Mekhilef. "High performances of grid-connected DFIG based on direct power control with fixed switching frequency via MPPT strategy using MRAC and neuro-fuzzy control." Journal of Power Technologies96.1 (2016): 27.

[22] Abdelmalek, Samir, Hocine Belmili, and Smail Toufik. "Robust Advanced Control Power Based on Vector Control Approach."

[23] Valipour, Khalil, and Reza Najafi. "Performance Evaluation of Doubly-Fed Induction Generator Using Combined Vector Control and Direct Power Control Method." Indonesian Journal of Electrical Engineering and Computer Science 3.1 (2016): 49-58.

[24] Mohammadi, Jafar, et al. "A combined vector and direct power control for DFIG-based wind turbines." IEEE Transactions on Sustainable Energy 5.3 (2014): 767-775.

[25] Badihi, H., Zhang, Y., & Hong, H. (2015). Wind turbine fault diagnosis and fault-tolerant torque load control against actuator faults. *IEEE Transactions on Control Systems Technology*, *23*(4), 1351-1372.

[26] Habibi, H., Yousefi Koma, A., & Sharifian, A. (2016). Power and velocity control of wind turbines by adaptive fuzzy controller during full load operation. *Iranian Journal of Fuzzy Systems*, *13*(3), 35-48.

[27] Kim, Y. M. (2016). Robust data driven H-infinity control for wind turbine. *Journal of the Franklin Institute*, *353*(13), 3104-3117.

[28] Giger, U., Kühne, P., & Schulte, H. (2017). Fault Tolerant and Optimal Control of Wind Turbines with Distributed High-Speed Generators. *Energies*, *10*(2), 149.

[29] Jafarnejadsani, H. (2013). *L1-Optimal Control of Variable-Speed Variable-Pitch Wind Turbines* (Doctoral dissertation, University of Calgary).

[30] Jafarnejadsani, H., Pieper, J. K., & Ehlers, J. (2013). Adaptive Control of a Variable-Speed Variable-Pitch Wind Turbine Using Radial-Basis Function Neural Network. *IEEE Trans. Contr. Sys. Techn.*, *21*(6), 2264-2272.

[31] Habibi, H., Nohooji, H. R., & Howard, I. (2017, December). Constrained control of wind turbines for power regulation in full load operation. In *Control Conference (ASCC), 2017 11th Asian*(pp. 2813-2818). IEEE.

[32] Lan, J., Patton, R. J., & Zhu, X. (2018). Fault-tolerant wind turbine pitch control using adaptive sliding mode estimation. *Renewable Energy*, *116*, 219-231.

[33] Sloth, C., Esbensen, T., & Stoustrup, J. (2011). Robust and fault-tolerant linear parameter-varying control of wind turbines. *Mechatronics*, *21*(4), 645-659.

[34] Aissaoui, A. G., Tahour, A., Essounbouli, N., Nollet, F., Abid, M., & Chergui, M. I. (2013). A Fuzzy-PI control to extract an optimal power from wind turbine. *Energy conversion and management*, *65*, 688-696.

[35] Kühne, P., Pöschke, F., & Schulte, H. (2018). Fault estimation and fault-tolerant control of the FAST NREL 5-MW reference wind turbine using a proportional multi-integral observer. *International Journal of Adaptive Control and Signal Processing*, *32*(4), 568-585.

[36] Abdelmalek, S., Azar, A. T., & Dib, D. (2018). A novel actuator fault-tolerant control strategy of DFIG-based wind turbines using Takagi-Sugeno multiple models. *International Journal of Control, Automation and Systems*, *16*(3), 1415-1424.

[37] Simani, S., Farsoni, S., & Castaldi, P. (2015). Fault diagnosis of a wind turbine benchmark via identified fuzzy models. *IEEE Transactions on Industrial Electronics*, *62*(6), 3775-3782.

[38] Habibi, H., Nohooji, H. R., & Howard, I. (2017). Power maximization of variable-speed variable-pitch wind turbines using passive adaptive neural fault tolerant control. *Frontiers of Mechanical Engineering*, *12*(3), 377-388.

[39] Tabatabaeipour, S. M., Odgaard, P. F., Bak, T., & Stoustrup, J. (2012). Fault detection of wind turbines with uncertain parameters: a set-membership approach. *Energies*, *5*(7), 2424-2448.

[40] Habibi, H., Rahimi Nohooji, H., & Howard, I. (2017). Optimum efficiency control of a wind turbine with unknown desired trajectory and actuator faults. *Journal of Renewable and Sustainable Energy*, *9*(6), 063305.

[41] Cho, S., Gao, Z., & Moan, T. (2018). Model-based fault detection, fault isolation and fault-tolerant control of a blade pitch system in floating wind turbines. *Renewable Energy*, *120*, 306-321.

[42] Habibi, H., Nohooji, H. R., & Howard, I. (2017, December). A neuro-adaptive maximum power tracking control of variable speed wind turbines with actuator faults. In *Control Conference (ANZCC), 2017 Australian and New Zealand* (pp. 63-68). IEEE.

[43] Bianchi, F. D., Sánchez-Peña, R. S., & Guadayol, M. (2012). Gain scheduled control based on high fidelity local wind turbine models. *Renewable energy*, *37*(1), 233-240.

[44] Qi, Y., & Meng, Q. (2012). The application of fuzzy PID control in pitch wind turbine. *Energy Procedia*, *16*, 1635-1641.

[45] Habibi, H., Nohooji, H. R., & Howard, I. (2018). Adaptive PID control of wind turbines for power regulation with unknown control direction and actuator faults. *IEEE Access*, *6*, 37464-37479.

[46] Savaghebi, M., Jalilian, A., Vasquez, J. C., & Guerrero, J. M. (2012). Secondary control for voltage quality enhancement in microgrids. *IEEE Transactions on Smart Grid*, *3*(4), 1893-1902.

[47] Boukhezzar, B., & Siguerdidjane, H. (2011). Nonlinear control of a variable-speed wind turbine using a two-mass model. IEEE Transactions on Energy Conversion, 26(1), 149-162.

[48] Basu, A. K. (2013). Microgrids: Planning of fuel energy management by strategic deployment of CHP-based DERs–An evolutionary algorithm approach. *International Journal of Electrical Power & Energy Systems*, *44*(1), 326-336.

[49] Taher, S. A., & Bagherpour, R. (2013). A new approach for optimal capacitor placement and sizing in unbalanced distorted distribution systems using hybrid honey bee colony algorithm. *International Journal of Electrical Power & Energy Systems*, *49*, 430-448.

[50] Chandrasekaran, K., & Simon, S. P. (2012). Multi-objective unit commitment problem with reliability function using fuzzified binary real coded artificial bee colony algorithm. *IET generation, transmission & distribution*, *6*(10), 1060-1073.

[51] El-Zonkoly, A. M. (2013). Multistage expansion planning for distribution networks including unit commitment. *IET Generation, Transmission & Distribution*, *7*(7), 766-778.

[52] Marzband, M., Azarinejadian, F., Savaghebi, M., & Guerrero, J. M. (2017). An optimal energy management system for islanded microgrids based on multiperiod artificial bee colony combined with Markov chain. *IEEE Systems Journal*, *11*(3), 1712-1722.

[53] Maleki, A., & Askarzadeh, A. (2014). Artificial bee swarm optimization for optimum sizing of a stand-alone PV/WT/FC hybrid system considering LPSP concept. Solar Energy, 107, 227-235.

[54] Roy, K., Mandal, K. K., & Mandal, A. C. (2016). Modeling and managing of micro grid connected system using Improved Artificial Bee Colony algorithm. International Journal of Electrical Power & Energy Systems, 75, 50-58.

[55] Moghaddam, M. M., Marzband, M., & Azarinejadian, F. (2017, May). Optimal energy management for a home Microgrid based on multi-period artificial bee colony. In Electrical Engineering (ICEE), 2017 Iranian Conference on (pp. 1446-1451). IEEE.

[56] Karaboga, D. (2005). An idea based on honey bee swarm for numerical optimization (Vol. 200). Technical report-tr06, Erciyes university, engineering faculty, computer engineering department.

[57] Karaboga, D., & Basturk, B. (2007). A powerful and efficient algorithm for numerical function optimization: artificial bee colony (ABC) algorithm. Journal of global optimization, 39(3), 459-471.

[58] Abedinia, O., Wyns, B., & Ghasemi, A. (2011, May). Robust fuzzy PSS design using ABC. In Environment and Electrical Engineering (EEEIC), 2011 10th International Conference on(pp. 1-4). IEEE.

[59] Gitizadeh, M., Khalilnezhad, H., & Hedayatzadeh, R. (2013). TCSC allocation in power systems considering switching loss using MOABC algorithm. Electrical Engineering, 95(2), 73-85.

[60] Tiacharoen, S., & Chatchanayuenyong, T. (2012). Design and development of an intelligent control by using bee colony optimization technique. American Journal of Applied Sciences, 9(9), 1464.

[61] Awan, S. M., Aslam, M., Khan, Z. A., & Saeed, H. (2014). An efficient model based on artificial bee colony optimization algorithm with Neural Networks for electric load forecasting. Neural Computing and Applications, 25(7-8), 1967-1978.

[62] Abedinia, O., Naslian, M. D., & Bekravi, M. (2014). A new stochastic search algorithm bundled honeybee mating for solving optimization problems. Neural Computing and Applications, 25(7-8), 1921-1939.

[63] Safavi, M. (2013). Application of ABC algorithm for grid-independent hybrid hydro/photovoltaic/wind/fuel cell power generation system considering cost and reliability. International Journal of Renewable Energy Research (IJRER), 3(4), 928-940.

[64] Oliva, D., Cuevas, E., & Pajares, G. (2014). Parameter identification of solar cells using artificial bee colony optimization. Energy, 72, 93-102.

[65] Babar, B., & Crăciunescu, A. (2014, April). Comparison of artificial bee colony algorithm with other algorithms used for tracking of maximum power point of photovoltaic arrays. In International Conference on Renewable Energies and Power Quality (ICREPQ'14) Cordoba (Spain), 8th to 10th April.

[66] soufyane Benyoucef, A., Chouder, A., Kara, K., & Silvestre, S. (2015). Artificial bee colony based algorithm for maximum power point tracking (MPPT) for PV systems operating under partial shaded conditions. Applied Soft Computing, 32, 38-48.

[67] Baraean, A. M., & Al-Duwaish, H. N. (2018, April). Coordinated Design of a Fuzzy Logic Power System Stabilizer and an SVC-based Stabilizer for Single-Machine Infinite-Bus Power System. In 2018 5th International Conference on Control, Decision and Information Technologies (CoDIT) (pp. 464-469). IEEE.

[68] Masuda, S. (2014). A Model Reference Adaptive Control Based on On-line Frit Approaches Using a Normalized Recursive Least Square Method. IEEJ Transactions on Electronics, Information and Systems, 133(10), 1950-1956.

[69] Wakasa, Y., Tanaka, K., & Nishimura, Y. (2012). Online controller tuning via FRIT and recursive least-squares. IFAC Proceedings Volumes, 45(3), 76-80.

[70] Wakasa, Y., & Adachi, S. (2015). Fictitious reference iterative tuning considering input saturation. IEEJ Transactions on Electrical and Electronic Engineering, 10, S159-S161.

Vitae

Personal Information:

- Name: Ali Ameen Ali Balfas
- Nationality: YEMENI
- Address: Seiyun – Hadhramout – Republic of Yemen
- Date of Birth: 18th October 1986
- Email: ali.a.balfas@hotmail.com
- Mobile: (+967) 730554715
- Home phone: (+967) 5428282
- Place of Birth: Hadhramout – Republic of Yemen
- Marital Status: Married

Education:

- MSc (Electrical Engineering), 2019
    - College of Electrical engineering
    - King Fahd University of Petroleum and Minerals
    - Dhahran, Saudi Arabia
- BSc (Electronic and Communication), 2012
    - College of engineering
    - Hadhramout University of Science and Technology
    - Al-Mukalla, Hadhramout, Republic of Yemen

Training Courses:

- Courses in Microsoft office 2010 (Windows7 – Word – Power point – Excel – Internet – Access) during the year 2012 provided by Ahqaf institute, Seiyun, Hadhramout, Republic of Yemen.
- Courses in English language "general English" (January – May 2006) provides by Modern American Language Institute MALI, Aden, Republic of Yemen.

- Courses in English language "preparing of TOEFL" (March – August 2013) provides by Aa-to-Zz English Academy, Success English Academy and ValuePoint English Academy, Bangalore, India.
- Transmission Course (PCM – PDH – SDH) during the month of July 2010 at the General Telecommunication Institute (GTI), Sana'a, Republic of Yemen.
- Summer training at Yemen Mobile Corporation in Sana'a on July to August 2010.
- Computer devices maintenance (Hardware – Software) 2010, Provided by Ahqaf institute, Seiyun, Hadhramout, Republic of Yemen.
- Mobile maintenance (Hardware – Software) 2013, Provided by Computer Science Center, Seiyun, Hadhramout, Republic of Yemen.
- Course in adobe photoshop 2014, Provided by Computer Science Center, Seiyun, Hadhramout, Republic of Yemen.

Skills:

- Language Skills
  - Arabic – native
  - English – (working knowledge)
- Computer software programs such as Microsoft Office (Word – PowerPoint - Excel), the internet and matlab
- Ability to work under pressure
- Ability to work with work group